Apatone® induces endometrioid ovarian carcinoma (MDAH 2774) cells to undergo karyolysis and cell death by autoschizis

Gilloteaux, Jacques; Lau, H. Lee; Gourari, Ioulia; Neal, Deborah; Jamison, James M.; Summers, J. L.

Published in:
Translational Research in Anatomy

DOI:
10.1016/j.tria.2015.10.005

Publication date:
2015

Document Version
Publisher's PDF, also known as Version of record

Translational Research in Anatomy 1 (2015) 25–39

Contents lists available at ScienceDirect

Translational Research in Anatomy

journal homepage: http://www.journals.elsevier.com/translational-research-in-anatomy

Research article

Apatone® induces endometrioid ovarian carcinoma (MDAH 2774) cells to undergo karyolysis and cell death by autoschizis: A potent and safe anticancer treatment

Jacques Gilloteaux [a, c, *], H. Lee Lau [a], Ioulia Gourari [a], Deborah Neal [b], James M. Jamison [b], J.L. Summers [b]

[a] Department of Anatomical Sciences, St George's University International School of Medicine, KB Taylor Scholar's Program, Northumbria University, Newcastle upon Tyne, WI, NE1 8ST, United Kingdom
[b] The Apatone Development Center, St Thomas Hospital, Summa Research Foundation, Akron, OH 44310, USA
[c] Unité de Recherche en Physiologie Moléculaire (URPhyM), Faculté de Médecine, Université de Namur, Belgium

ARTICLE INFO

Article history:
Received 27 August 2015
Received in revised form
22 October 2015
Accepted 22 October 2015
Available online 23 November 2015

Keywords:
Ascorbate
Menadione
Endometrioid ovarian cancer MDAH 2774
Autoschizis cell death
DNA

ABSTRACT

Ovarian cancers are still the most lethal gynecologic malignancy. As a novel strategy against this poor outcome cytotoxic alterations induced by a pro-oxidant treatment on human ovarian endometrioid carcinoma (MDAH 2774) cells are revisited by using light, scanning and transmission electron microscopy. A series of sequential and concomitant cellular and organelle injuries induced by ascorbate: menadione combination (VC: VK_3) or Apatone® is emphasized. This adjuvant or treatment is able to kill majority of these tumor cells through 'autoschizic cell death', a mode of cell death different than apoptosis. Autoschizic cell death is significant after a short period of treatment to decrease the ovarian tumor cell population through induced injuries that proceed from membranes to most organelles: karyolysis with nucleolar segregation and fragmentation, autophagy of mitochondria, lysosome and other organelles as well as cytoskeletal defects. The cytoskeletal damages are evidenced by morphology changes that included auto- or self-excised pieces of cytoplasm lacking organelles apparently facilitated by grouping of vacuolated endoplasm. These results obtained against this endometrioid ovary cell line are comforted by other studies using Apatone® against other carcinomas in vitro and in vivo. Altogether these reports support Apatone® as a new drug that can favorably be used as a novel potent, safe, and inexpensive clinical adjuvant or treatment against ovarian cancers.

1. Introduction

In the United States alone, the number of estimated new ovarian cancer cases for 2015 is estimated as 21,290 with an outcome of 44% survival, i.e. an estimated 14,180 deaths [1]. Even though this figure represents about 3% of all new female cancer cases which is lower than the marked incidence 12 years ago [2], the current statistics have remained similar during the past 45 years. It is also noted that ovarian cancer is more common in North America and Europe than in Africa and Asia [3–6].

Due to its late detection, and lack of clear screening guidelines, ovarian carcinomas are the most lethal malignancies. Its poor survival rate can be attributed to vague, non-specific clinical signs and markers signaling the disease. In addition, its slow and insidious peritoneal invasiveness that is difficult to assess with only by a few routine, clinical markers. Poor ovarian carcinomas' treatment outcomes are caused by detection at an advanced stage; after installment of the malignant cells on the peritoneal surfaces of one or more organs, very similarly to what is found prostate tumors [7]. Additionally, these cancers spread early through lymphatics and it is only long-surviving patients where haematogenous, metastatic spreads result in bone marrow or brain infiltrations [8]. The 5-year survival rate of all ovarian cancers is estimated to be around 30% after treatment [9]. This rate has not improved for the last 35 years [10,11]. Thus, ovarian cancer is truly the leading cause of death among women with the traditional gynecologic malignancies in the United States [12] and elsewhere [6]. Furthermore, chemotherapy

* Corresponding author. Department of Anatomical Sciences, St George's University International School of Medicine, UNN – Life Sciences, Drill Hall 013, Newcastle upon Tyne, NE1 8ST, United Kingdom.
E-mail address: jgilloteaux@sgu.edu (J. Gilloteaux).

http://dx.doi.org/10.1016/j.tria.2015.10.005

against any ovarian cancers reveals its poor clinical outcome because of its chemo-resistance.

This basic science report complements previous reports despite the development of new markers and more specific treatment [13–21]. Morphology, histochemistry and biochemistry data from Apatone® treatment of MDAH2774 human endometrioid ovarian carcinoma cells may be safely translated into clinics as a complementary, alternative medical adjuvant or even primary treatment in early detection.

This report again brings credence to support the usage in clinics of an innovative, potent, safe and inexpensive treatment, made from a combined ascorbate: menadione sulfite, named Apatone®. This drug can become an adjuvant to surgical, irradiation and/or chemotherapeutic treatment against ovarian carcinomas, related perineal and peritoneal malignancies. Alone Apatone® kills tumor cells efficiently not only in vitro but also tumors bearing in vivo xenotransplants [21–23]. In combination with irradiation, it offers an attractive complementary chemotherapeutic therapy that leaves normal cells and other organ-systems unaffected by the treatment [21,22,24].

2. Materials and methods

2.1. Cell line

Human ovarian carcinoma cells (MDAH 2774), purchased from the American Type Culture Collection (ATCC, Rockville, MD), originate from the ascite's fluid of a patient with endometrioid ovarian carcinoma who did not received chemotherapy or radiation prior the collection of cancer cells. Characterized at the MD Anderson Hospital and Tumor Institute (Houston, TX), these cells were found to be hypotriploid [25]. This cell line was cultured in Eagle's Minimum Essential Medium (MEM; Gibco Labs, Grand Island, NY) supplemented with 10% heat-inactivated fetal bovine serum (FBS; Gibco) and 50 μg/ml gentamicin sulfate (Sigma Chem. Co, St Louis, MO). All incubations, treatments and microtiter tetrazolium (MTT) assays were performed at 37 °C and with 5% CO_2 unless other conditions are stated.

2.2. Test solutions

Ascorbate sodium (Vitamin C or VC) and menadione bisulfite (VK_3), purchased from Sigma Chemical Company (St. Louis, MO), were used for the cytotoxicity experiments. The vitamins were dissolved in phosphate-buffered saline (PBS) to create 8000 μM VC, 500 μM VK_3 and 8000 μM VC: 80 μM VK_3 test solutions. Both vitamins were dissolved in culture medium to create test solutions with final concentrations of 2032 μM VC, 20.32 μM VK_3, and 2032 μM VC: 20.32 μM VK_3. To prevent photo-degradation of the vitamins, vitamin solution preparation and all experiments were performed in a darkened laminar flow hood.

2.3. Cell culture

Titer dishes were seeded with 1.0×10^6 MDAH cells; they were allowed to attach and spread for 24 h at 37 °C. Following exposure to each vitamin alone and in combination, cells were harvested at one-, two-, and three-hour intervals and processed for TEM observations. In this report tumor cells Sham- or Control-treated were compared with the combined VC: VK_3-treated cells.

2.4. Cytotoxicity assay

The cytotoxicity assay was performed using the microtetrazolium [MTT 3-(4, 5-dimethylthiazol-2-yl)-2, 5-diphenyldiphenyl tetrazolium bromide] assay as described previously [23]. After vitamin treatment and the incubation period, cytotoxicity was evaluated using the MTT assay. Following linear regression, the line of best fit was determined and the 50% cytotoxic dose (CD_{50}) was calculated.

2.5. Histochemistry

Circular coverslips were seeded with 10^5 MDAH cells and incubated for 24 h at 37 °C. The cells were then overlaid for one-, two-, and three-hour with media containing only media (Sham-treated group) and their combination as VC: VK_3. All cells were washed twice with PBS, fixed for 1 h in formalin at room temperature and then washed three times for 5 min/wash with PBS. Feulgen DNA staining was accomplished according to Pearse [26] without other counterstaining. After rinsing, dehydration in graded ethanol, the preparations were cleared in xylene before mounted in synthetic DPX medium. Control slides that were not hydrolyzed nor treated by Schiff after hydrolysis did not provide staining of the chromosomes of dividing cells nor the DNA. All chemicals (at least 99% purity) were prepared and used from the same containers and originated from Fisher Scientific Co (Pittsburgh PA). Staining was accomplished simultaneously for both cover slips with treated cell groups to avoid batch specific variations in DNA degraded staining [27]. All dehydration and preparations were also made at the same time and in the same hood with light intensity and temperature (17–18 °C). After a 2-h setting to allow polymerization of mounting medium and to prevent light defects, all sections were stored in the dark at 4 °C overnight and examined the next day morning at the same time. Micrographs were taken under immersion oil with an Olympus BX51 photomicroscope (Olympus America, Melville, NY). All micrographs were printed from Kodak Ektachrome 64T reversal film (Kodak, Eastman Kodak Co, Rochester, NY) and prints were made from slides by using same batch of paper and photographic reagents.

2.6. Cell measurements

Cell size was determined using the orthogonal diameters method of Song et al. [28]. Briefly, the length was defined as the largest diameter, while the width was obtained by measuring the diameter of the cell orthogonally to the length. At least 100 cells were measured for each treatment group.

2.7. Densitometry of Feulgen staining data and statistical analysis

Optic densitometry of Feulgen stained samples was obtained and copied from Gilloteaux and collaborators [19]: nuclei observed in about 36 fields of color micrographs from each Sham and VC: VK_3-treated MDAH cells. The measurements of optical reflectance units were averaged in a histogram with standard error of the mean (s. e. m.). Repeatable measurements were able to be obtained within 1% of each reading. Following one-, two- and three-hour vitamin exposures, DNA degradation with the VC: VK_3 combination was assessed by measuring decreased intensity of Feulgen staining of tumor cell DNA compared with those obtained with Sham treated cells. The other measurements reported previously were made after either VC or VK_3 treatment alone and were compared with the ones reported here [19]. Two-way analysis of variance was used in which both vitamin treatments were interacted. The single-degree-of-freedom interaction test of the effect of the combination of VC and VK_3 followed directly from this two-factor model.

2.8. DNA gel electrophoresis

Total DNA was extracted after each treatment from 4.10^6 MDAH cells, run on 0.6% agarose gel treated according to [28] and stained with ethidium bromide as described in Ref. [19].

2.9. Scanning electron microscopy (SEM)

After each treatment, cells were washed with PBS and fixed in 2.5% glutaraldehyde phosphate buffered solution with 0.13 M sucrose; pH 7.35 or PBS for 10 min at room temperature according to [29]. After 2 × 10 min washes in sucrose-phosphate buffer, cells were post fixed in a 1% OsO_4 aqueous solution for 30 min at room temperature. Cells were then washed twice for 10 min in the same buffered solution before they were dehydrated and critical-point dried in a E-300 BioRad unit (Cambridge, MA). All samples were sputter-coated with gold-palladium to a thickness of 1.0–1.5 nm. Cells were then examined in a Hitachi S-570 SEM (Mountain View, CA) at 12–13 kV emission accelerating voltage and at a distance of 12–15 mm from the cells. Micrographs were collected with Polaroid type 55 films. Samples were viewed at 0 and at 35–40° tilt angles to obtain polar (cell size measurements) and profile views of the cells.

2.10. Transmission electron microscopy (TEM)

MDAH 2774 cells grown as a monolayer were exposed either to PBS alone or the VC: VK3 combination for 1 h, then washed in PBS buffer, harvested and allowed to sediment by slow centrifugation (450–500 rev/min). After removal of the supernatant, the treated cells were fixed in 2.5% phosphate-buffered glutaraldehyde solution with 0.13 M sucrose-phosphate, pH 7.35 for 30 min at room temperature in 2 mm^3 microfuge tubes [29]. After two 10-min washes in sucrose-phosphate buffer and gentle sedimentation of a formed pellet of cells for each treatment, 30 min post fixation was done in 1% osmium tetroxide aqueous solution, under a fume hood, and at room temperature. Pellets contrasted by this post fixation were washed twice for 10 min in the same buffered solution before dehydration and processing into PolyBed epoxy resin (Polysciences, Warrington, PA). From each blocks, one-μm thick sections were then stained in toluidine blue to select areas for ultramicrotomy. These sections were collected on 75- and 100-mesh hexagonal copper grids (SPI, West Chester, PA), stained in uranyl acetate and lead citrate, and examined in a Zeiss EM-10 TEM (Carl Zeiss, Thornwood, NY). The digitized images were obtained using an analySIS 2.1 software system © (Soft Imaging System GmbH, Lakewood, CO and Münster, Germany) in the Pathology Department of the Children's Hospital Medical Center of Akron, OH.

3. Results

Observations made with morphological techniques (SEM, LM and TEM) are described in the order the investigators collected data and complement those submitted in previous publications. This report emphasizes data comparing Sham-treatment against the VC: VK_3 combined treatment (Apatone®) to demonstrate that the cytotoxic injuries kills ovarian endometrioid carcinoma cells, further supporting its translating clinical potential.

3.1. SEM views

A general aspect of the preparations collected with this technique showed an even distribution of cells on the cultivation support with spaces caused by the arrest of culture long before cells attain their confluence. At first glimpse, MDAH cells distribute into a homogeneous population of small sized cells, ovoid to spherical and with a slight elongated morphology. They can flatten and display a poor contrast against their growing support. Their nuclear zone is elevated and often present with one elongated extension that resembles a cytoneme, giving them an oblong, stretched profile. Some cells can be noted with a large spherical profile compared to the elongated ones as they likely correspond to being less motile as they prepare to or have undergone replication. Other scant but obvious 'double' or 'twin' cells, still closely adjacent, can be found among this population and seem to corroborate this latter interpretation (Fig. 1A). Finally, Fig. 1C, a higher magnification of a field of Fig. 1A, verifies the general aspects of the Sham cells as they display upper cell surfaces loosely wrinkled that could be referred with a 'peau d' orange' texture with a few poorly preserved microvilli but bear a radiating and diffuse array of delicate filopodia (1–3 μm long) along their edges. In general, cells are ovoid to round and vary from 25 to 35 μm in length, 15–25 μm in width and sometime can show a single, uropod-like and short lamellipodia issued from their surfaces of culture support (Fig. 1A–B). In Fig. 1A tumor cells appear evenly spaced with a few overlapping cells suggesting some limited cell contact inhibition likely due to the culture time that was stopped when the cells were still separated from one another. Arising from a few cells one can notice short to long uropod- or cytoneme-like extensions running toward other cells. In the higher magnification (Fig 1B), several cells out of the previous Fig. 1A reveal their evenly textured surfaces, somewhat wrinkled like orange skin caused by appearing short digitations or short lamellipodia being flattened as they cover the upper surfaces of the cultivation support. They display similar size compared to those viewed on the basal aspects, revealing short size ranging from 0.5 to 1.0 μm in length. Tenuous filopodia (1–3 μm in length) can also be seen sprouting out of these lamellipodia in a loose but evenly distributed fan-like irradiated manner. Using light microscopy, most 1 μm-thick epoxy sections of pellets obtained after treatment (Fig. 2A–B) allowed complementary aspects with the morphology obtained with the SEM micrographs (Tables 1 and 2).

3.2. LM observations

3.2.1. Control or sham-treated MDAH 2774 cells

Using 1 μm-thick sections stained with Toluidine blue LM samples of culture areas of Sham MDAH 2774 tumor cells reveal some diversity in staining characteristics because diverse blue-to-purplish contrast appear. Sham cell population of MDAH 2774 is uninucleate, show high replication activity and growth in vitro. A few, rare multinucleate cells can be seen, as noted earlier (Gilloteaux et al., 2004). One has noted that most pale-stained cells in the micrographs of the pane in Fig. 2 are captured undergoing preprophase to anaphase stages and some obvious mitotic stages, eventually displaying chromosomes while those with highest contrast are in interphase. The interphase cells displayed a typical morphology characteristic of poorly differentiated tumor cells, showing a high nuclear: cytoplasmic ratio. Their shape and nuclei are sub-spherical and all of them displayed a large, prominent nucleolus, sometimes with a branching aspect as one can detect more than one sections of the nucleolar body (Fig. 2B). Similarly, in Fig. 4A and B, higher magnifications illustrate their surfaces that are not smooth and in most cells discrete and hairy aspects seem to confirm the many small lamellipodia better revealed with SEM technique. Furthermore, some uropodial-like extensions can be infrequently noted, such as in the insert of Fig. 4 A. It is noteworthy indicating that Sham cells reveal a densely contrasted cytoplasm. In addition, one can seldom observe tiny cell debris (less than 1.0 μm). Among the Sham cells in culture, entosis can be seldom observed as a cannibalistic activity where old or dying cells are captured and

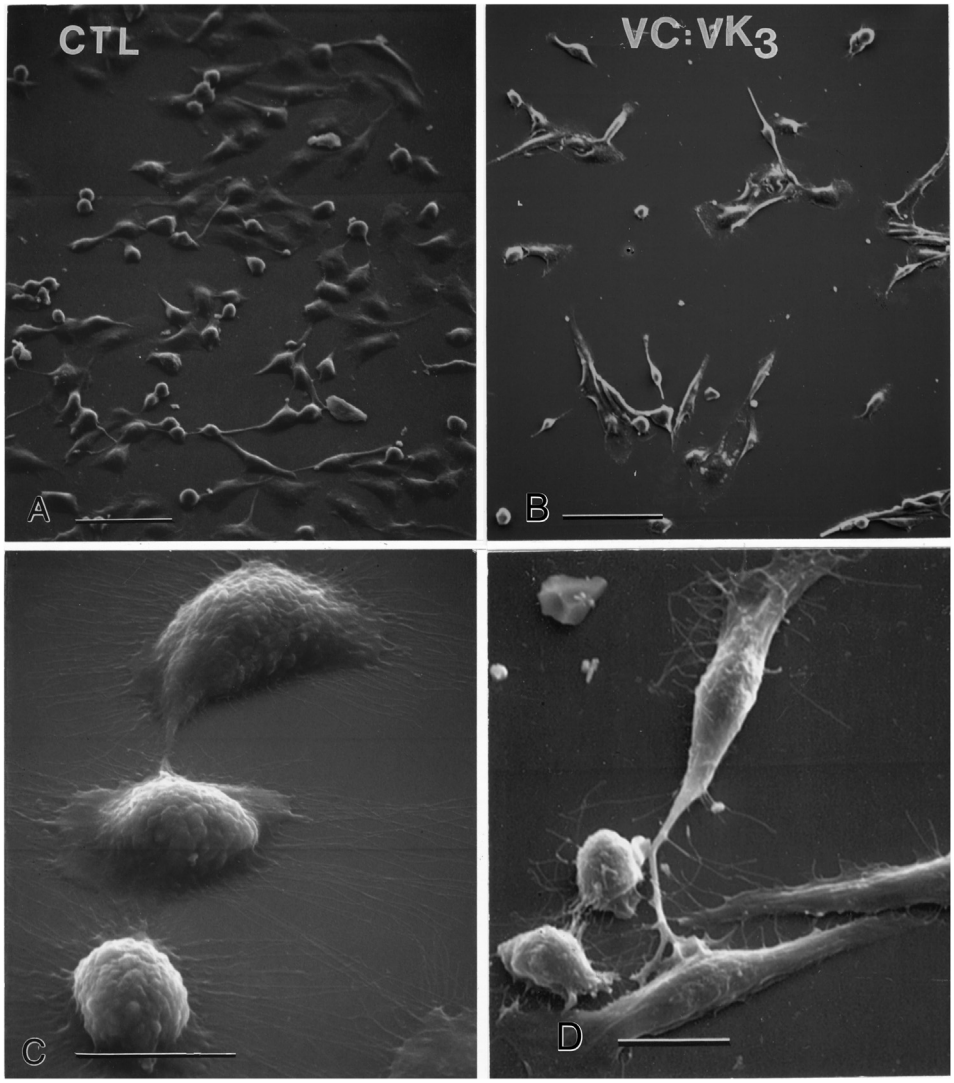

Fig. 1. A-D. SEM views of 1 h Sham-treated human ovarian carcinoma (MDAH 2774) cells on culture support. In A, a low magnification view of the evenly-distributed population of the pleomorphic cells adhering to their culture substratum. B, C and D show tumor cells at progressively higher magnifications demonstrating a surface, smoothly wrinkled and from their basal aspects sprout a few, short lamellipodia out of which at their basal aspects from which sprout numerous delicate long and short irregular filopodia sprouting out of lamellipodia. Scale in A is 50 μm, in B and C is 10 μm and in D is 1 μm.

recycled by more 'aggressive' young ones (Fig. 4A).

3.2.2. VC: VK_3-treated MDAH 2774 cells

A quick survey of several fields of view clearly verifies that these treated MDAH cells remain with obvious large, empty spaces of an outlived population of cells when compared with Sham-treated cells. These surviving cells are mainly elongated cells, appearing almost as fibroblast-like, with a spherical to oblong oval shape nuclei. The cells show long, tapered edges contacting one another or not with edges presenting crawling lamellipodia out of which numerous filopodia (1.0–3.0 μm) are issued. The cells rarely appear in clusters and, among them, a few spherical ones, often distorted, leave intercellular spaces littered by scattered corpses or cell debris (Fig. 1B). Along and adjacent to their cell surface a few, self-excised, cytoplasmic pieces with their delicate connections (<1.0 μm wide) can be found as contrasting from the background (Fig 3C and insert). The spherical cell type resembles those found in Sham cells but less contrasted and often possess several bulging or bursting blebs, again suggestive of cells undergoing self-cuts as shown in most micrographic fields of view (Fig. 3B and C). A few multinucleate cells, with 2–9 nuclei, stand by their enormous size among the populated preparation (Fig. 3A and C).

Endometrioid tumor cells in selected high magnified LM views of one-μm thick epoxy sections stained by toluidine blue clearly confirm the pleiomorphic alterations caused by the pro-oxidant treatment (Figs. 3 A–C and 5 A–B). Most spherical cells become elongated and distorted, with tapered aspect at one or both ends and often include extensions resembling cytonemes as lamellipodia. These structures are uniformly contrasted by a light to deep purple–violet hue according to their accumulated content in glycogen and, especially, in ribonucleoproteins. At first glance, cells appear difficult to size but through measurements they are smaller than the Sham cells with diameters ranging from less than 5–12 μm resulting in a calculated average diameter of 14.7 ± 3.8 μm after 1 h treatment that decreased to 12.8 ± 2.4 μm after 2-h treatment and to approximately 10.8 ± 1.3 μm after 3-h treatment. Some large cells display vacuolated cytoplasm and blisters while most undergo cytoplasmic self-cuts detected throughout the fields of view. Self-cuts are suggested by cells that appear spherical with their nucleus rimmed by a continuous but narrow layer of heterochromatin

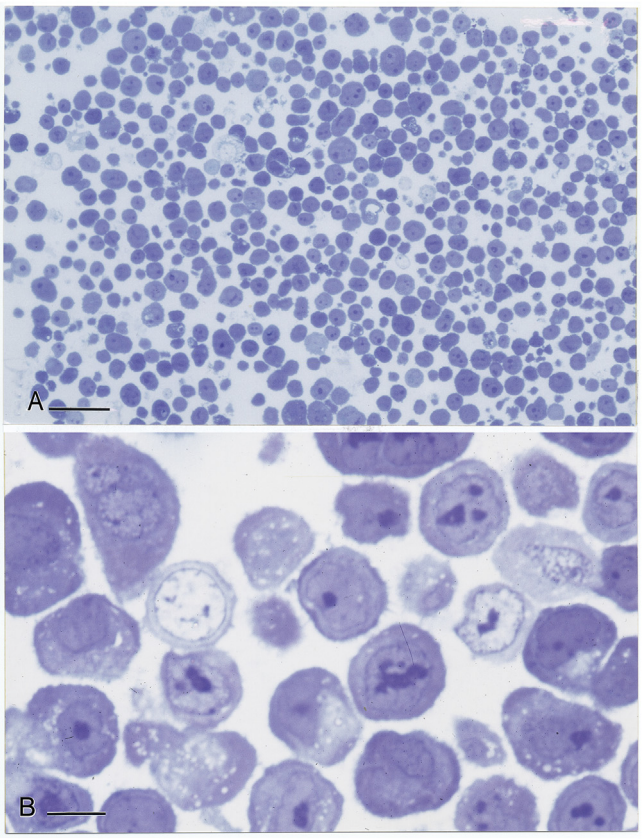

Fig. 2. A–B. Light microscope view of 1 h Sham treated human ovarian carcinoma (MDAH 2774) cells; toluidine blue stained epoxy 1 μm-thick sections. Most cells appear round cells with large spherical and indented nuclei; stages of mitosis are apparent in the palest cells. In B, a peculiar, multi-nucleated cell with spherical nucleoli in each nucleus and a closely adjacent, small cell with same contrast can be found. In C, examples of pale cells (labeled ' * ') undergoing pro-metaphase of cell cycle; a curved arrow marks an uropod and at its left a twin-cell is preserved in telophase. In D, a small arrow points to entosis in progress. The scale in A is 50 μm, in B is 10 μm.

Table 1
Diameters of MDAH 2774 cells and cell debris (in μm).

	Control	VC + VK_3
Length	25 – 35	9 – 15
Width	15 – 20	5 – 12
Cell debris	0.1 – 0.5	1.5 – 6.5

Measurements were taken with polar views of SEM and made on at least 100 cells or pieces of cell debris.

Table 2
Percent of population of MDAH 2774 undergoing mitotic replication and cell death after each treatment.

Treatment	Mitosis	Type of cell deaths		
		Oncosis	Apoptosis	Autoschizis
Control (n = 541)	7.2 ± 2.6[a]	1.3 ± 0.6	3.5 ± 0.6	2.7 ± 0.5
Vitamin C + K_3 (n = 717)	7.0 ± 2.1[b]	1.9 ± 0.2	3.0 ± 0.5	43.0 ± 6.5

[a] All stages of mitosis were detected.
[b] Only Prophase or Metaphase stages of mitosis were detected. The number of mitoses and number of each type of cell death were counted from at least 3 sets of thick sections and expressed as the average ± the standard error of the mean.

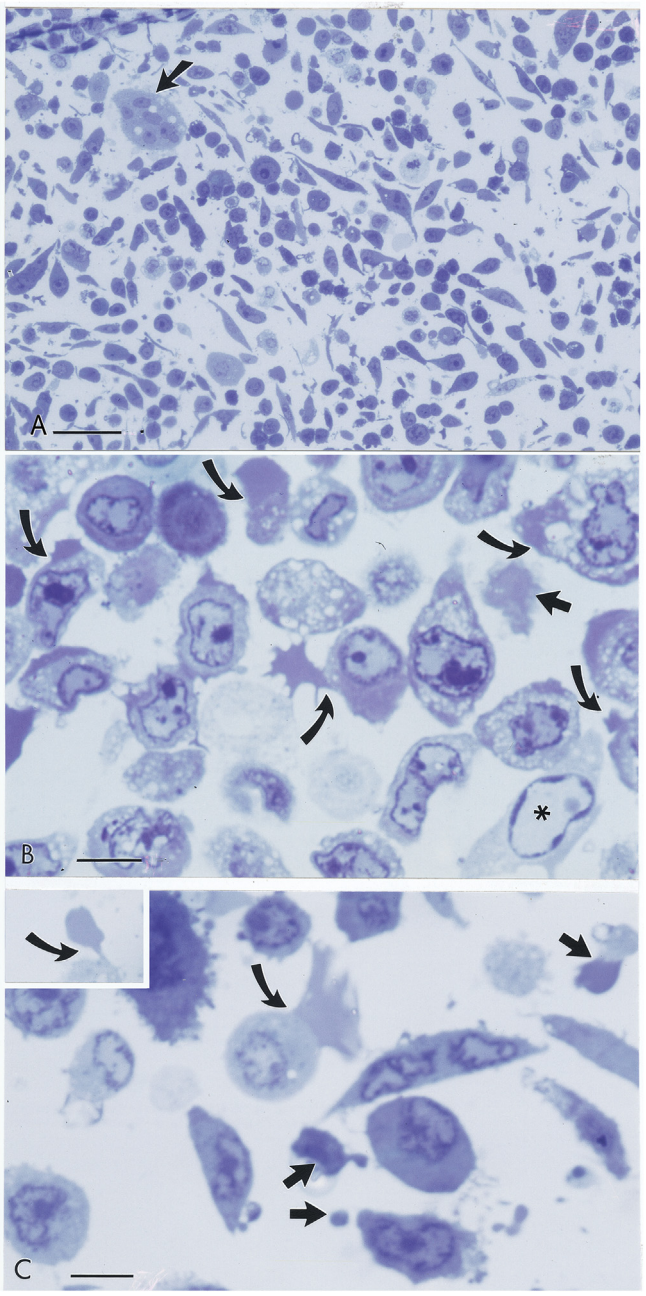

Fig. 3. A–C. LM views of 1 h VC:VK_3 -treated human ovarian carcinoma (MDAH 2774) cells; 1-μm thick epoxy section stained by toluidine blue. In A: cells show great pleiomorphism oblong and distorted cells and debris of cells in their intercellular spaces. Only a few spherical cells remain and those left are often much smaller than the Sham-treated cells. In B and C: Magnified views display most tumor cells surfaces show uneven texture and distorted nuclei and bubbly, vacuolated cytoplasm, making them less contrasted than Sham-treated cells. Small to enormous, round to conical, chubby blisters or blebs (curved arrows) appear along each cell suggesting alterations of the superficial and deep cytoskeleton. As a result, many debris litter the intercellular spaces (thick arrow in C). The scale is 50 μm in A, 10 μm in B in C.

and a narrow perikaryon that hangs on a small to large, uniformly pinkish-blue to dark purple cytoplasmic piece that appears to also self-cut (i.e. insert of and in Fig 3C and star-labeled in Fig. 5A and B). Among the cells treated and collected, numerous 0.5–6.5 μm diameter cell debris can be noticed and viewed in the intercellular spaces. In many cells the nucleoplasm appears peculiarly pale pink

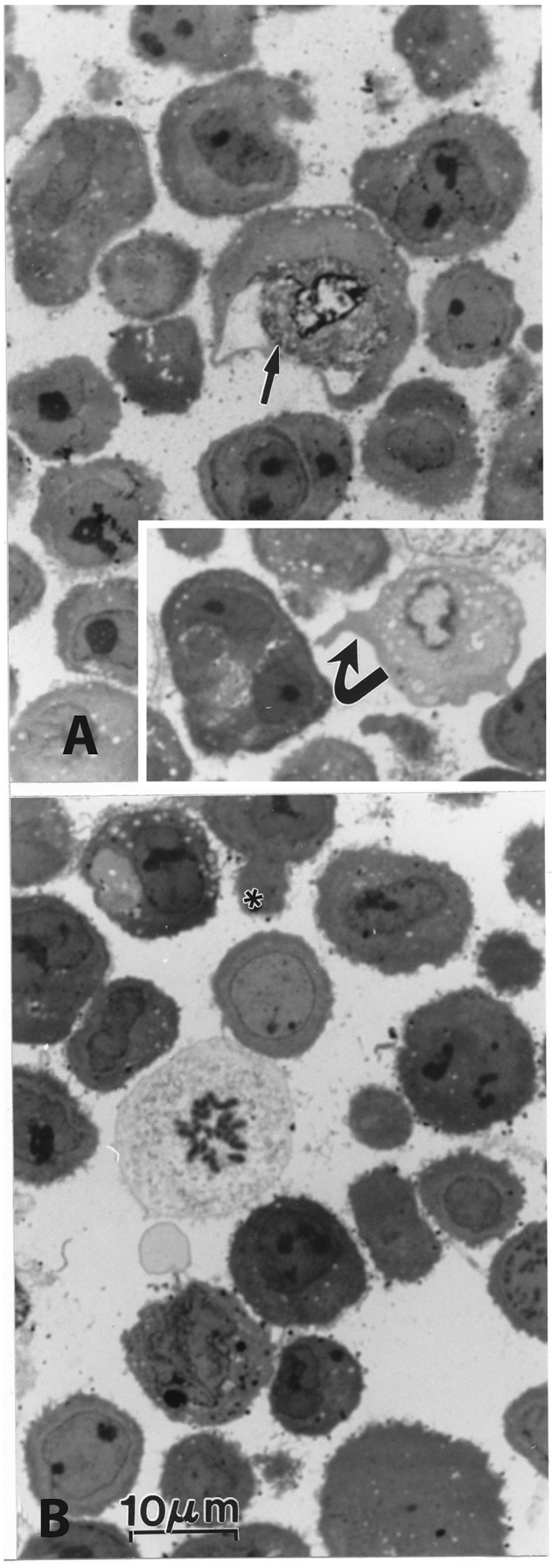

with a 'milky' hue view with peripheral heterochromatin patches displayed as thickened curved rims along the inner membrane. In other treated cells, the *quasi* entire heterochromatin seems extracted out of the nucleus, leaving tiny peripheral bits (Figs. 3 B–C, 5 A–B). Only very rarely treated cells display a huge spherical and pyknotic nuclear mass that precedes necrosis (Fig 5A–B). Many of the treated cells also reveal distorted nuclei indicative of cytoskeleton alterations. Other nuclear changes show nucleoli reduced to their compacted granular component into either one huge round to irregularly oblong contrasted mass or fragments often reduced into a minute spherical dot less than 0.5 μm in diameter (Figs. 3 B–C, 5 A–B). In many cases the nucleoli that remain or eventually fragment into irregularly oblong or spherical bodies can appear in the intercellular spaces after cell demise among the other remaining injured, poorly surviving cells. Among the collected population, only a few, rare treated cells undergo cell death through apoptosis as indicated by their nucleus with highly contrasted masses (arrowed in Fig 5A and B).

3.3. Histochemistry

3.3.1. Feulgen stain

This technique verifies that DNA degraded through karyolysis caused by the combined VC: VK_3 treatment (Fig 6). One-, two and three-hour duration Sham (CONT-treatment tumor cells) show intact and heavy stained chromatin. The same pane compares an adjacent photomontage of samples of tumor cells after one-, two- and three-hour duration treatment with VC: VK_3 that shows a significant decrease, not only of cell size and shape, but also a significant diminished nuclear contrast indicating a significant depletion in DNA compared to Sham cells, as noted in the histogram of Fig. 7. In addition, Fig. 8 depicts the data obtained with one agarose gel electrophoresis after 3-h treatment by VC: VK_3-MDAH cells. It displays a smear pattern when compared with intact fibroblasts suggesting a DNA fragmentation that is certainly different than the laddering degradation of DNA found in apoptosis. After VC: VK_3 treatments, the Feulgen stain demonstrates a significant decrease in the intensity of the staining contrast suggestive of increased karyolytic damages in accordance to the duration of treatment (Figs. 6–7). This prompted repetitious DNA total extractions and viewing them with gel electrophoresis.

3.3.2. DNA gel electrophoresis

The possibility that total DNA degraded in MDAH cells occurred out of treatment is unlikely since human foreskin fibroblasts (MHRF) exposed to both Sham-Control and after 4-h treatment with the vitamin combination did not show such damages. DNA extracted and resolved electrophoretically shown in Fig. 8 demonstrates that lanes 2 and 3 respectively contain the DNA of VC: VK_3-treated (VCK) and Sham-treated (CNT) MHRF cells. DNA from the Sham-treated MHRF cells appears as a single high molecular weight band slightly below the well in which it was loaded. Conversely, DNA from VC: VK_3-treated MHRF cells appear as a low molecular weight smear at or below 200 bases. On the opposite side, DNA extracted from sham-treated MDAH cells appears as a

Fig. 4. A and B. LM views of human endometrioid carcinoma (MDAH 2774), 1-μm thick epoxy section stained by toluidine blue, 2-h after Sham-treatment. All cells display spherical aspects with surfaces covered by short 'hairy' microvillar-like extensions. Some cells show an uropod-like (curved arrow in insert of A) and eventually undergoing cell cycle (also in insert of A) as noted by harboring chromosomes either in prophase or pale and in pre-metaphase (in A and B). Large vacuole-like areas made of accumulated glycogen and fatty deposits along with few cell blebs or debris can be seen (*). Surprisingly, one entosis phenomenon is captured in A (small arrow). Scales are 10 μm.

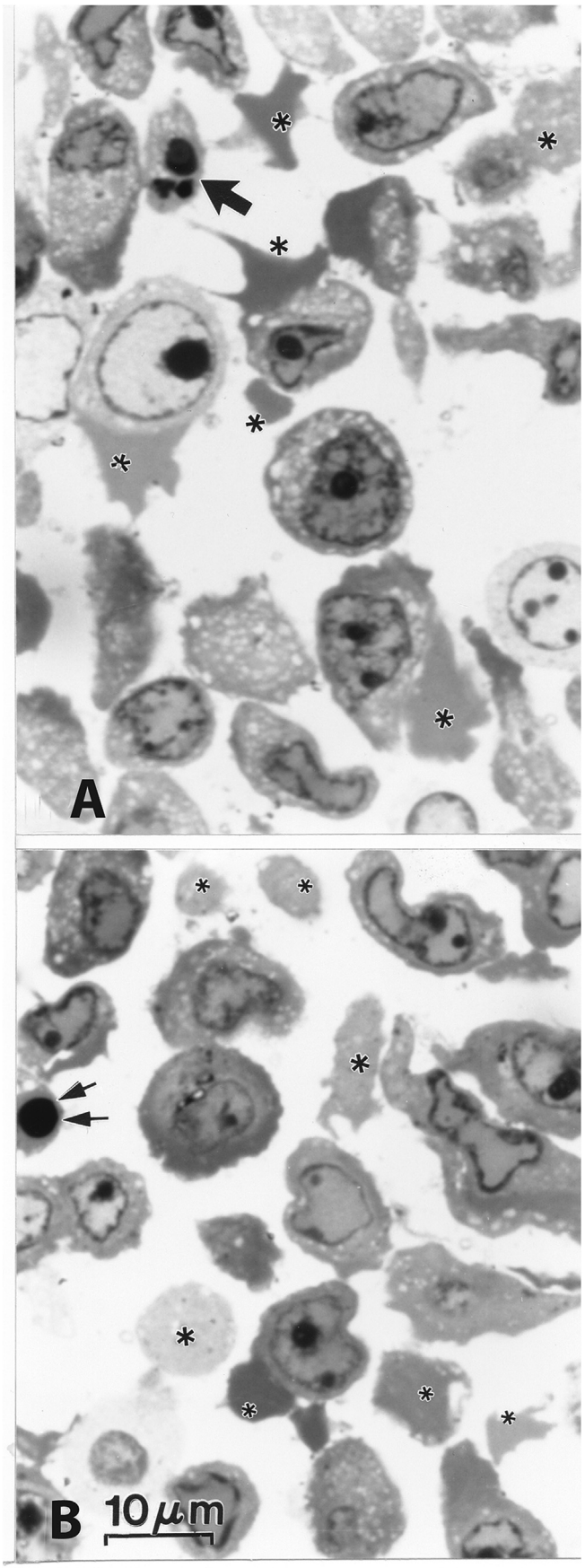

single high molecular weight band slightly below the well in which it was loaded, while the DNA from vitamin treated MDAH cells exhibits a spread pattern. The absence of laddering in the vitamin-treated lanes with DNA damages strongly suggests that VC: VK_3 treatment induced cell death through a different process than in classic apoptosis.

3.3.3. *Densitometry measurements*

In order to quantify the changes in staining patterns that suggested karyolysis wherein significant DNA degradation was expected, we measured differences in light absorption between treatments (Fig 8). Measurements of the DNA in nuclei of the treated MDAH cells as displayed were made only after a 3-h vitamin exposure due to the abundance of cell death, detachment and disintegration in longer vitamin exposures. As shown in the histogram of Fig. 8, DNA staining intensity of Sham-treated (CONT cells) is 32.5 ± 1.127. The DNA staining intensity values for VC and VK_3 alone are 21.6 ± 1.127 and 32.6 ± 1.127 [14,18], while the DNA staining intensity of the vitamin combination is 15.6 ± 1.127. Notice that the average DNA level following VK_3 appears to look similar to the Sham group. By contrast, DNA level following VC or VC: VK_3 treatment is significantly lower than in the control group ($p < 0.0001$). In addition, DNA intensity level following VC: VK_3 treatment is significantly different from the DNA intensity level only following the VC treatment ($P < 0.03$). The standard error values are all identical because they were based on a pooled variance estimate (Fig. 8).

3.4. *TEM aspects: (Figs. 9 and 10A–G)*

Control or Sham-treated MDAH 2774 cells always display a spherical morphology that ranged between 20 and 35 μm in diameter; they are covered by small microvilli-like filopodia, ranging between 1 and 1.5 μm, often with an unusual bifurcate aspect (Fig 9). These endometrioid cells are poorly differentiated with a typical high nuclear: cytoplasm ratio and contain a large nucleolus. With TEM, the large nuclei often shows ovoid to subspherical shape with a deep indent as a narrow groove that makes the organelle to appear 'coffee bean' in morphology. This is often detected with thick views or sections of histology fields of view. Because of its large size, only the edge of the intranuclear branching structure of the nucleolus is usually detected. The overall nucleoplasm is euchromatic with the delicate thickening of the inner nuclear membrane being clearly interrupted by nuclear pores. The perikaryal, narrow cytoplasm is filled by innumerable ribonucleoprotein granules with patches of glycogen and a few fatty droplets. A number of rough and smooth endoplasmic cisternae are distributed throughout the remaining cytoplasm.

Some MDAH2774 tumor cells defects observed with LM after treatment by the combined, pro-oxidant vitamins (Apatone®) are shown in the pane of Fig. 10A–G. There a selected series of micrographs that demonstrates some of the ongoing auto- or self-excising (autoschizic) processes and degradations at the level of the nucleus, other organelles and cytoskeleton. The damages observed with the vitamin combination are exacerbated and occur more rapidly (1 h vs. 3 h) than with an individual vitamin

Fig. 5. A and B. LM views of human endometrioid carcinoma (MDAH 2774), 1-μm thick epoxy section stained by toluidine blue, 2-h after VC: VK_3 treatment. Most cells show elongated and distorted shapes along with their nuclei. If spherical, the nucleus appear empty of chromatin or with remnants of heterochromatin as patches on the inner nuclear membrane. Most nucleoli are resolved as either enormous, condensed spherical or fragmented masses of fragments. Most cells display ongoing self-excisions that contain contrasted ribonucleoprotein material and their debris that result (*). A few, rare cells undergo apoptosis (arrows). Scales are 10 μm.

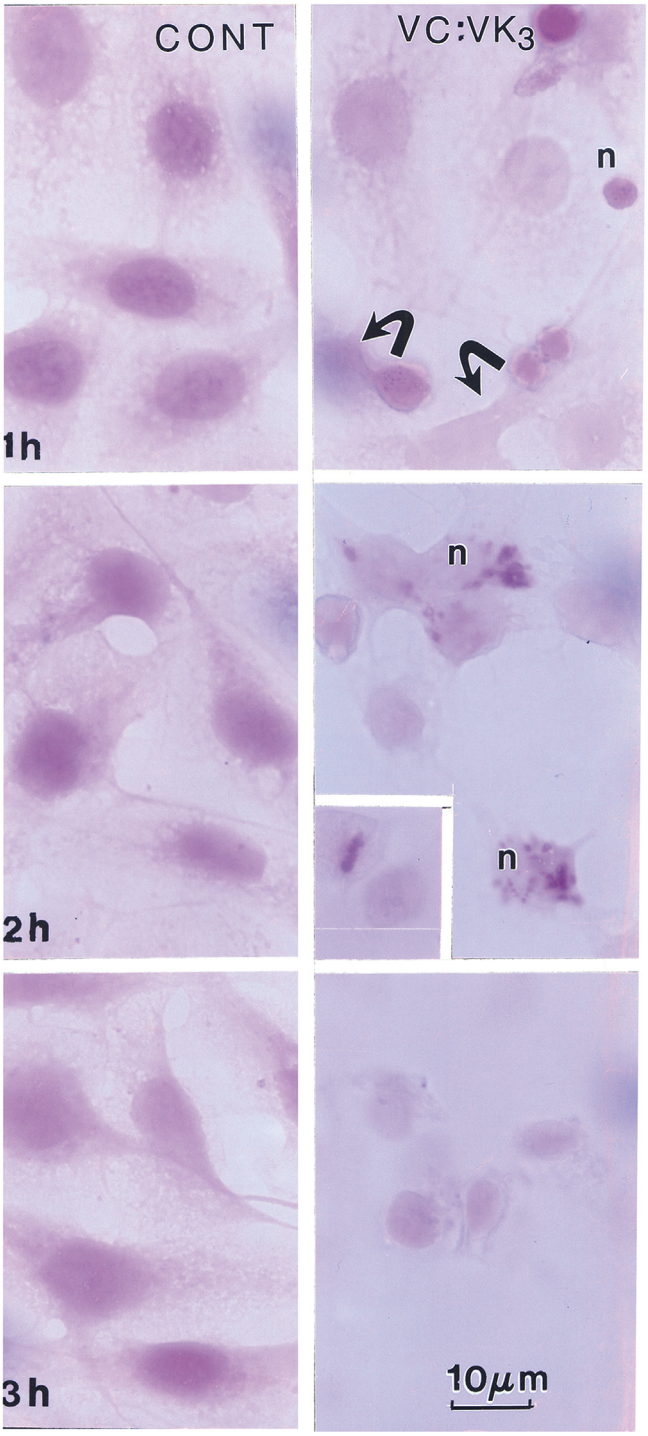

Fig. 6. Feulgen-stained Sham-and VC: VK_3 -treated ovarian (MDAH2774) endometroid carcinoma cells. The gallery of micrographs contains columns (period of treatments: 1-, 2-hr, and 3-hr) and rows (type of treatments: Sham (CONT) and combined VC-VK_3. In all the micrographs, "n" represent the nucleus. Note that chromosomes block in metaphase are clearly viewed in the 2-h treatment insert. Small curved arrows mark selected examples of cytoplasmic self-excisions. The scale indicated as 10 μm is for all the illustrations of Sham and treated cells. Reprint from part from our published work [18].

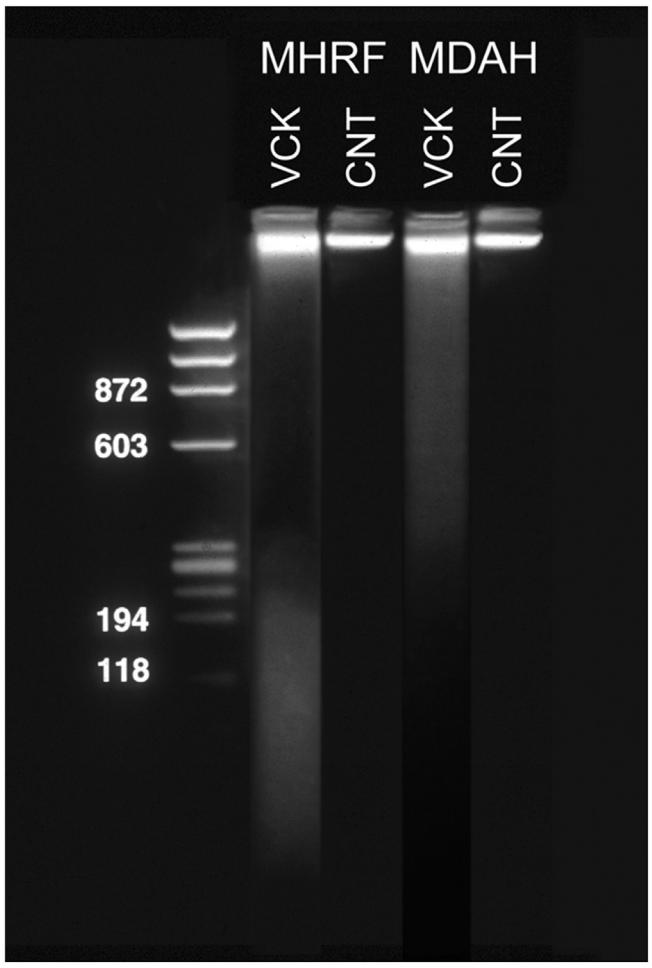

Fig. 7. Agarose gel electrophoresis of total DNA from Sham-treated and VC: VK3 treated human fibroblasts (MHRF) and ovarian endometroid (MDAH 2774) cells. Lane 1 contains molecular weight markers. Lane 2 contains DNA from VC: VK3- MHRF treated cells (VCK) while lane 3 contains DNA from Sham-treated MHRF cells (CNT). Lane 4 contains DNA from VC: VK3-treated MDAH cells (VCK) while lane 5 contains DNA from Sham-treated MDAH cells (CNT). By permission [18].

treatment, as previously tested [13,15,17–20]. Nuclear damages accumulated with nucleolar changes involving chromatin illustrate that the heterochromatin is roughly plastered along the inner nuclear membrane (seen with LM in Fig. 3A). Additionally, the condensation of the nucleolus results in ribonucleoprotein masses where chromatin can be seen in some sort of clouds-like pattern afar of them as depicted in Figs. 3C and 5A–B. At the same time, a diminished cell size caused by auto-cuts (or autoschizis) verifies karyorrhexis while segregating a large piece of cytoplasm to further excisions is displayed in Fig. 10A–G. Throughout the treated cells most mitochondria appear swollen with a fine granular content amongst one or more osmiophilic clumped membrane debris in their matrices. Most other organelles are unable to be resolved as they were degraded as small to large vacuoles where only some large or small osmiophilic bodies can be resolved throughout the cytoplasm, clumped along and in the perikaryal areas (Fig. 10A and C).

Accumulated vacuoles of the swollen SER-RER assemble in the perikaryon where other damaged organelles group or align along the most contrasted peripheral zones. They appear to assume some sort of self-excision in these uniformly contrasted pieces of cytoplasm loaded with ribonucleoproteins and glycogen. These self- or auto-cuts contribute to the tumor cell excisions, hence diminishing their size. An example of elongated cell through cytoskeletal damage is best exemplified in Fig. 10D–G where the insert reveals a constellation of gathered vacuolated bodies that likely undertake the excising cell process we have previously named autoschizis.

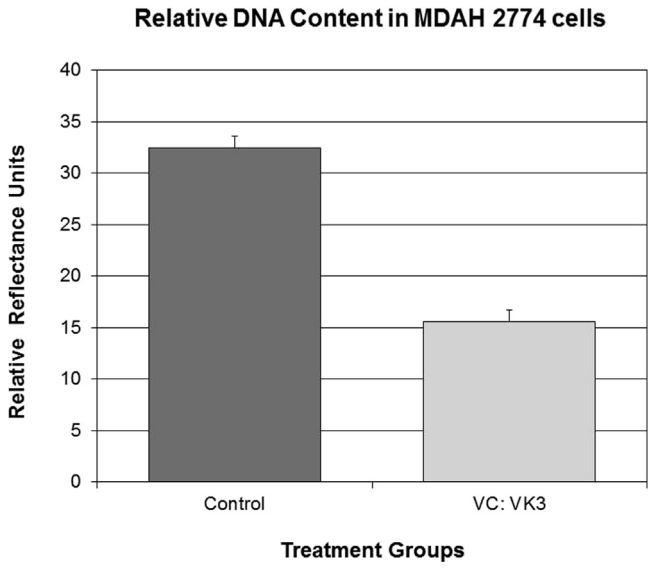

Fig. 8. The histogram summarizes the relative DNA content of Sham- and VC:VK3-treated endometrioid (MDAH 2774) cells. The bars correspond to the calculated averages of the densitometric measurements of the reflectance intensity collected from the microscopic preparations as some selected fields of view are illustrated in Fig. 7.

4. Discussion

4.1. The cell line

MDAH 2774 is an endometrioid ovarian adenocarcinoma cell line developed from ascite cells from a female patient with endometrioid ovarian cancer; it forms tumors in nude mice with triploidy of 1, 2, 3, 6, 11, 12, 16, X, and a single copy or monosomy of number 17 and number 21 chromosomes. Chromosome 5 was triploid in 6 out of 7 cells while the remaining chromosomes showed apparent random variation in the number of copies with a general trend toward triploidy [25].

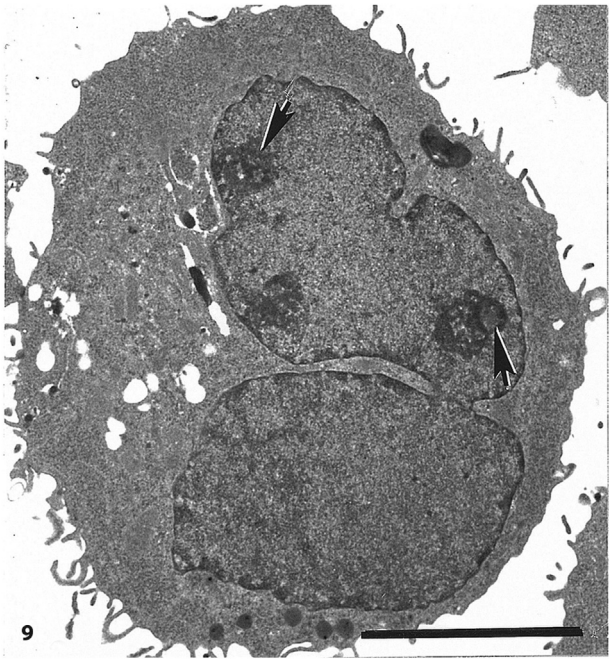

Fig. 9. TEM view of a small Sham-treated endometrioid (MDAH 2774) cell depicting its large coffee bean-shaped nucleus and its small cytoplasm crowded by electron densely contrasted ribonucleoproteins and containing a few fatty deposits and a few contrasted round lysosomes can be noticed in the lower cell area. A branching nucleolus appears in this section. Scale equals 5 μm.

4.2. Endometrioid carcinoma of the ovary

Even though the etiology of ovarian cancers is poorly understood reproductive hormones are likely involved estrogens and metabolites, especially estrone, as well as exogenous hormones or factors and may include progestins or factors, including replacement therapies and infertility treatments can be involved in the ovarian cancers as supported by studies in animals [31–33].

Endometrioid carcinoma cells of the ovary have been described by several authors as endometrium-like (for example, but not limited to [34–42]). A classic interpretation describes that some serous endometrioid tumors, usually serous in nature, may have an entwined and dualistic origin: (i) with the germinal epithelium (i.e. the main ovarian mesothelial surface epithelium in many cases) [34,43] and (ii) with the endometrial deposits or implants as the appellation 'endometrioid' suggests [43–49]. This tumor type is often associated with carcinoma of the uterine corpus that has been reported as high as 20% of cases [34,43,50,51]. Other endometrioid tumors can arise with papillomavirus infection and decreased expression of p16 out of hypermethylation of the promoter or the gene [52,53]. A constant finding of laminin α1 in basement membrane, not found in serous or mucinous ovarian type, could be marker of this endometrioid tumor type while a lack of laminin α2 and collagen type VII immunoreactivity were also noted in endometrioid carcinomas of the ovary [54]. Finally, another study showed that endometrioid carcinomas were likely vimentin positive and carcinoembryonic antigen positive contrarily to the endocervical endometrioid that has these markers negative [55]. Additional defects incurred caused by genome alterations in common with other carcinomas, such as E-cadherin changes [56–58].

Endometrioid tumor can be highly aggressive, usually present in postmenopausal age [59], and found in advanced stages. They comprise of serous, high-grade benign cancer cells but can become easily malignant due to their epigenetic mutations to acquire Müllerian characteristics with cell shape modifications, appearance of E-cadherin, secretory mucins (MUC1, MUC2, MUC3 and MUC4) and CA125 (such as [41,60,61]). Using DNA microarrays for assessing ovarian cancer gene expression 150 out of 35,000 genes associated with ovarian defects with a highest frequency in TP53 mutation along with other genetic profiling [62]. Its subtypes have an associative plethora of 422 gene mosaic mutations [63,64]. In addition, hormones, growth factors and cytokines are involved in initiating and progressing growth along with some hereditary predisposition that can play an important role (review in Ref. [41]). Within the most recent survey genetic alterations can cause 10% of all ovarian cancers [5]. In all, ovarian endometrioid tumors such as MDAH 2774 can include – but are not limited to – gene defects TP53, Stat 3, ARIDIA, BRCA1, BRCA2, HER2, PIK3CA, deletion of tumor suppressor genes PTEN with K-ras transformation, NF1, RAD51B can also be found in chemoresistant serous ovarian defects, and common with mucous and clear cell ovarian tumor types [65–67]. In addition to receptors for estrogens, progesterone and androgen those gene defects can be used as markers in ovarian carcinomas [69,70]. Furthermore, BRCA1 and BRCA2 gene defects that include loss of their promoter methylation, can account only for 3–13% of all resistant ovarian cancers [69,71]. They can co-associate with non-polyposis colorectal cancer Lynch syndrome, mutations of mismatch repair [NMR] genes [72]. Finally, out that of

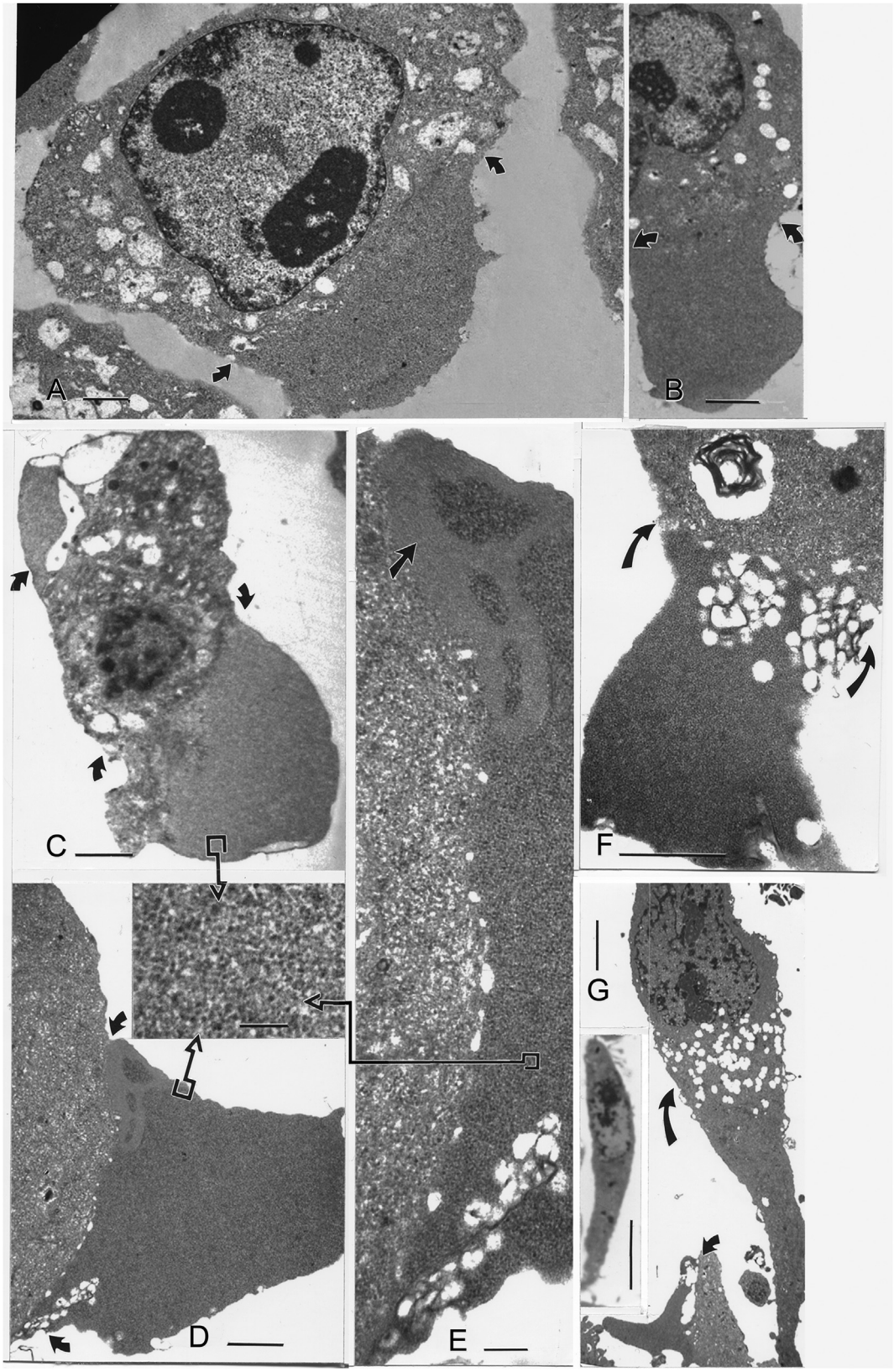

Fig. 10. A–G: This pane is a series of TEM aspects of VC: VK3-treated endometrioid ovarian carcinoma (MDAH 2774) cells and confirming their LM injuries with cell morphology changes including nuclei (A, C, and G) and cytoplasmic alterations leading to tumor cell autoschizis with cell distortions and autoschizic cell death. In A: a nucleus demonstrates compaction of the nucleolus into three masses of granular components (G < B <A)>. In C the nucleus undergoes karyorrhexis with fragmented chromatin. The self-excising cytoplasm cuts are highly contrasted with innumerable ribonucleoproteins and glycogen granules (shown in C -E regions enlarged). The approximate regions of auto-cuts are indicated by small curved arrows throughout the micrographs. They contain many aligned or grouped numerous vacuoles out of endomembrane (endoplasm) and mitochondria damaged by the pro-oxidant, anticancer treatment. Scales in all the micrographs equal 1 μm and in the one of enlarged pieces of C–D–E equals 200 nm.

65 gene libraries 2270 somatic mutations were identified as Tp53 in a majority of first surgeries while ATM, ATR, TOP2A and TOP2B were mutated in the entire data set. At second surgery, mutation data clustered patients in two groups characterized by different mutational profiles in genes associated with HR, PI3K, miRNA biogenesis and signal transduction [73].

4.3. The strategy of pro-oxidant treatment used against tumor cells

Initially conceived by Taper and collaborators [21,22,24,74–79] the pro-oxidant strategy against cancer cells is to favor a derepression of some part of the metabolome (macromolecular component, such as HP [69]), and enzyme repression or inhibition during activities in carcinogenesis (e.g. DNases and RNases, peroxidative and catalatic, NADPH reductase, etc). Such unfavorable changes in the metabolome of tumors allow for a potent cytotoxic activities because the tumor cells are known to have very low catalatic and peroxidase activities [80–84]. Hence a new therapeutic strategy of an alternative and complementary cytotoxic actions of a mixture of two natural products where the data have been provided by the aforementioned results and those discussed in the earliest published data [13,17–21].

4.4. VC: VK_3 treatment aka Apatone®

Taper and coworkers demonstrated that a co-administration of sodium ascorbate (vitamin C or VC) and 2-methyl-1,4-naphthoquinone (vitamin K3 or VK3) to a variety of carcinoma cell lines and xenotransplanted tumors in a VC: VK_3 ratio of 100:1 resulted in equivalent antineoplastic activity at concentrations that were 10–50 times lower than when either vitamin was administered alone [21,22,24,74–79,85,86]. Because tumors exhibit characteristic loss of some DNases and RNase activities [89,90], Taper's group further they hypothesized that these enzymes could be reactivated by a number of agents, including vitamins C and K_3 and, in the course of many published studies, showed that selective and sequential reactivation of DNase I by VK_3 (within 1 h after treatment) and DNase II by VC (3–4 h after treatment) when both vitamins were administered in combination, resulted in synergistic degradation of DNA and tumor regression [21,22,24,74–79]. These anticancer activities were caused by the redox cycling of the vitamins in the mechanism of action of the vitamin combination causing an oxidative stress. The induced production of reactive oxygen species (ROS) accompanied by a classical, concomitant damage to membranes and other lipid-rich cell structures, along with the oxidation of sulfhydryl (-SH) groups and depletion of reduced glutathione [87,88,90,91] produced irreversible damage in the cancer cells which leads to autoschizis [13–19,21,92]. These anticancer activities were illustrated in other cell lines and in xenotransplanted tumors [21,87,88,94,95].

4.5. The antiproliferative activity of the VC: VK_3 combination

The vitamin combination has been shown to exhibit synergistic in vitro antiproliferative activity against liver, endometrial, oral epidermoid, breast and a wide variety of human urologic tumor cell lines as well as in vivo against liver and prostate cancer [21,22,24,74–79]. At least a portion of this activity may be due to cell cycle arrest at G_1/S and G_2/M [94,95]. Multinucleate cells observed throughout the cultivation samples suggest disruptions of cell cycle at both stages aforementioned either through prophase or anaphase blocks. Additional cytotoxic activity is related to an increased rate of redox cycling and ROS production caused by the ability of VC to facilitate the single electron cycling of VK_3 [96–99]. Because of the redox cycling and ROS production of the vitamin combination, the homeostasis of the MDAH cells is more rapidly disturbed and the cytological insults are greater than with either vitamin alone.

Finally, the spread DNA pattern following electrophoresis (Fig. 2B) suggests that DNA degradation was not part of an apoptotic process. While these results are consistent with the sequential reactivation of both DNase I and II [21], they do not preclude the possibility that the decreased Feulgen staining may be related to ROS-induced DNA damage stemming from an increased rate of redox cycling. Therefore, additional experiments must be performed to unequivocally determine the trigger(s) and origin(s) of the molecular mechanism responsible for this DNA degradation.

In previous in vivo studies, sub-therapeutic doses of VC and VK_3 were administered to the test animals so that the vitamins only exerted their cytotoxic effects when both vitamins were present together in the tumor cells. Under these conditions, selective and sequential reactivation of DNase I by VK_3 and DNase II by VC in the vitamin combination, resulted in synergistic degradation of DNA and tumor regression [21,24,75,76]. To simulate these conditions in vitro and to ensure that we did not miss the window of activity and synergism, the vitamins were administered at concentrations where one vitamin alone (VC) was active, while the other vitamin (VK_3) was only marginally active. MTT cytotoxicity assays with the vitamins [23,92,93] produced CD_{50} values of 1528 μM for vitamin C, 41.8 μM for vitamin K_3 and 165 μM/1.65 μM for the VC: VK_3 combination. Therefore, the dose of VC used in the current study (2032 μM) was slightly greater than CD_{50} value of 1528 μM. To maintain VC: VK_3 ratio of 100:1, 20.32 μM VK_3 was used. Since the CD_{50} of VK_3 is 41.8 μM and the dose of VK_3 employed in this study is 20.32 μM, the activity of the VK_3 is expected to be much less than the activity of the VC. Indeed, VC treatment produced a significant decrease in Feulgen staining of DNA, while VK_3 treatment had little effect on Feulgen staining. However, when VK_3 is administered with VC, there was an additional significant decrease in Feulgen staining of DNA beyond what was observed for VC alone.

The intracellular mechanisms of favorable penetration in the tumor cells by the anticancer drug mixture is the possession of GLUT-1 expression in most ovarian tumors, including the endometrioid ones, because ascorbate can use this channel to accumulate in the tumor cells [100], especially after oxidative stresses created by a menadione or VK3 fast and first activity [21], that is why an apparent antioxidant such as ascorbate, becomes an oxidative species [90].

These results demonstrate that the CD_{50} value of the vitamin combination for the human foreskin fibroblasts (MHRF) fibroblasts was 6-fold greater than CD_{50} value of the vitamin combination for the MDAH cells. These results agree with those of Zhang and coworkers [101] who showed that while VC and VK_3 induced synergistic cytotoxicity against fibroblasts as well as tumor cells, fibroblasts were not as sensitive to the cytotoxic effects of the vitamins as the tumor cells. In addition, in the current study, the FIC values for the MDAH cells and the MHRF cells are nearly identical (0.147 vs. 0.145). These results suggest that once cytotoxic doses are reached in non-tumor cells, the vitamins exhibit the same type of synergistic toxicity observed in tumor cells. Since the CD50 value for VC: VK_3 treated MHRF cells was 1000 μM: 10.0 μM and the vitamins were administered at a dose of 2032 μM: 20.32 μM, one would expect to see some cytotoxicity in the fibroblasts. In fact, a low molecular weight smear is seen in Fig. 2B when total DNA of MHRF cells was examined.

The in vitro results suggest a very narrow therapeutic window for the vitamin combination. However, the results of in vivo studies demonstrated that administration of clinically attainable doses of oral vitamins could significantly reduce the growth rate of solid prostate cancer tumors in nude mice any significant bone marrow

toxicity, changes in organ weight or pathological changes of these organs [21,24].

4.6. Morphologic changes of tumor cells

The combined anticancer treatment resulted in showing by light microscopy techniques that MDAH cells have decreased their population, modified their general morphology through some likely defects in their superficial actin networks [13–17,102], and deep cytoskeleton of cytokeratin filaments and have also significantly reduced their size through self-excisions or autoschizis. Some of these injurious defects have also favored cell death through these damages as one also found nuclear changes that were already described when tumor cells underwent such cell death by autoschizis [13–20]. The least of all can be found as MDAH cells depicted a progressive but also significant DNA disintegration caused by the combined treatment strongly supporting the reactivation of DNAses favored by the treatment as it was supported for prostate and bladder carcinoma cells in vitro [13,19,92] and, in vivo, as xenotransplants [21,22,24]. Observing some large, bi-nucleated MDAH cells as a result of the combined treatment can also validate the anticancer treatment because our earliest data on other carcinoma cells, similarly treated, showed after flow cytometry that a blocks occurred in G1-S and G2-M phases backing up previous observations [94,95].

The fine structural micrographs also substantiate the injurious events induced by the treatment that favored auto- or self-excisions of the highly contrasted cytoplasm containing no organelles. Along with these events nuclei also depicted nucleoli without their associated chromatin. It is because the chromatin component withdrew from them and reduced those nucleoli into compact, ribonucleoproteins masses [13–20] as they also undergo a significant DNA degradation as noted by the diminution of the Feulgen stain contrast [18]. Simultaneously fibrillarin pattern has been altered [103]. This is similar to other carcinoma cells treated by this pro-oxidant mixture [92,104,105]. TEM views indicated that the treatment with VC: VK_3 favored injuries inflicted by ROS stresses on membranes and also included vacuolization and autophagic events [13–17,104,105] The perikaryal zones demonstrate only remnants of most organelles degraded through leaking lysosomes [92,105–108]. Meanwhile the most intriguing and interesting phenomenon already noticed in our earliest data are the auto- or self-excising events [13–20] that seemed to have deemed a grouping of these vacuoles at the edges of those perikaryal zones. In those areas, as shown in many illustrations, small SER/RER vacuoles (25–200 nm diam) appeared to join up, merge and create a weakness zone out of which piece(s) of cytoplasm can excised. Similar amalgamation of such event can also further continue to reduce cell size and with nuclear degradation. This is shown in other cell lines studied from which we derived the name of cell injury that progresses into a new mode of cell death, different than apoptosis, not only by its morphology but also its biochemical characteristics [13–20,105].

These auto- or self-excising events can be suggested by SEM collected data where pieces of cells or corpses scattered the intercellular spaces in all of our cell lines examined after the same treatment. This was also seen in human prostate carcinoma grafted in mice [21,92].

4.6.1. DNA degradation as karyolytic damages of MDAH2774

Ten DNA optic density measurements of MDAH 2774 cells were obtained within each of 3 independent sites on the microscopic preparations for each of the four conditions yielding 30 observations per experimental condition (Fig. 7). The analysis of variance modeled the nesting of measurement within site (mixed modeling) so that there were three primary units of analysis (sites) for each condition. A significance level of 0.05 was used for the interaction test. This was also reviewed in previous reports [13–20].

Total DNA extracted from MDAH-treated cells and human foreskin fibroblasts (MHRF) following Sham treatment or 4 h treatment with the vitamin combination. The DNA was then resolved electrophoretically as shown in Fig. 8. Lanes 2 and 3 contain the DNA of VC: VK_3-treated (VCK) and sham-treated (CNT) MHRF cells. The DNA from the Sham-treated MHRF cells appears as a single high molecular weight band slightly below the well in which it was loaded. Conversely, the DNA from VC: VK_3-treated MHRF cells appear as a low molecular weight smear at or below 200 bases. The DNA from Sham-treated MDAH cells also appears as a single high molecular weight band slightly below the well in which it was loaded, while the DNA from vitamin treated MDAH cells exhibits a spread pattern. The absence of laddering in the vitamin-treated lanes strongly suggests that VC: VK_3-induced cell death is not apoptosis. This indicates that tumor cells are damaged first with a sequence indicated as follows: VC: VK_3 > VK_3 > VC > Sham treatment. This sequence can be verified by the aforementioned experiments. A new mode of cell death by self-excising, not just cytoplasm but also the desintegration of DNA had also occurred

Here one evidenced with morphology and histochemistry as well as biochemistry techniques that one of the common ovarian carcinomas as other carcinomas, exposed to a pro-oxidant treatment of one-, two- and three-hour to a combined ascorbate: menadione mixture die mainly through autoschizis without damaging normal cells.

4.6.2. Autoschizis cell death

This mode of induced cancer cells is different that apoptosis as it is not programmed. Data showed that tumor cells die out of nucleases' reactivation accompanying by unprotected peroxidation with lysosomal damages leaking cathepsins to nucleus structures [105]. This mode of cell death has been characterized through several techniques that included biochemistry following the first observations made in 1995 [109] and, in the following years, similar data accumulated on human bladder, ovarian, prostate and murine prostate carcinomas [13–19,21,93–95,104,109] as well as reviewed in three book Chapters [20,92], including a more recent, [110], in press].

Autoschizis exhibits a unique set of morphological and biomolecular alterations that distinguish it from apoptosis and oncosis as defined in previous studies and surveys [13,14,19,20,92,104,106]. Specifically, in bladder and prostate cancer cells, cytoplasmic self-excisions and the associated nuclear changes result in the diminution of cell size, the disappearance of chromatin from nucleolus and nucleoplasm and subsequent nucleolar compaction and fragmentation during karyorrhexis and karyolysis. During these events, DNA is degraded in a random fashion similar to that occurring during necrosis.

Autoschizis, a new form of cell death, and histochemical changes suggests a potentially important ovarian cancer treatment: several trends are evident from this study. First, there is a significant decrease in the viable adherent cell population in the sequence Sham-Control > VC > VK_3 > VC: VK_3. Second, cell diameters decrease from 15-35 μm to 7–12 μm in the same sequence. Third, extreme pleiomorphism, cell damage, and progressive self-morsellation results from vitamin treatment in the order VC: VK_3 > VK_3 > VC > Sham-Control. Ultrastructural damages appear to correlate qualitatively with decreases in Feulgen staining (DNA content), self-morsellation and DNA damage in the sequence VC: VK_3 > VC > VK_3 > Sham-Control. Fourth, plasma membrane and intracellular membrane damage, extreme mitochondrial

defects, including swelling and some cytoskeletal defects increase ensues after vitamin treatment in the sequence VC: VK_3 > VK_3 > VC > Sham-Control. Fifth, progressive nuclear changes (from redistribution of euchromatin producing a thin margin of DNA along the nuclear envelope and dissolution) and nucleolar changes (from branching to compaction, segregation and crystallization of the ribonucleoproteins into a single round body) are seen following vitamin administration in the sequence VC: VK_3 > VK_3 > VC > Sham-Control. These injurious processes contribute to cell death by autoschizis which cell death after treatment by Apatone® or an appropriate mixture of VC: VK_3 is, for MDAH 2774 cells, more frequent than apoptosis or oncotic necrosis [15–18].

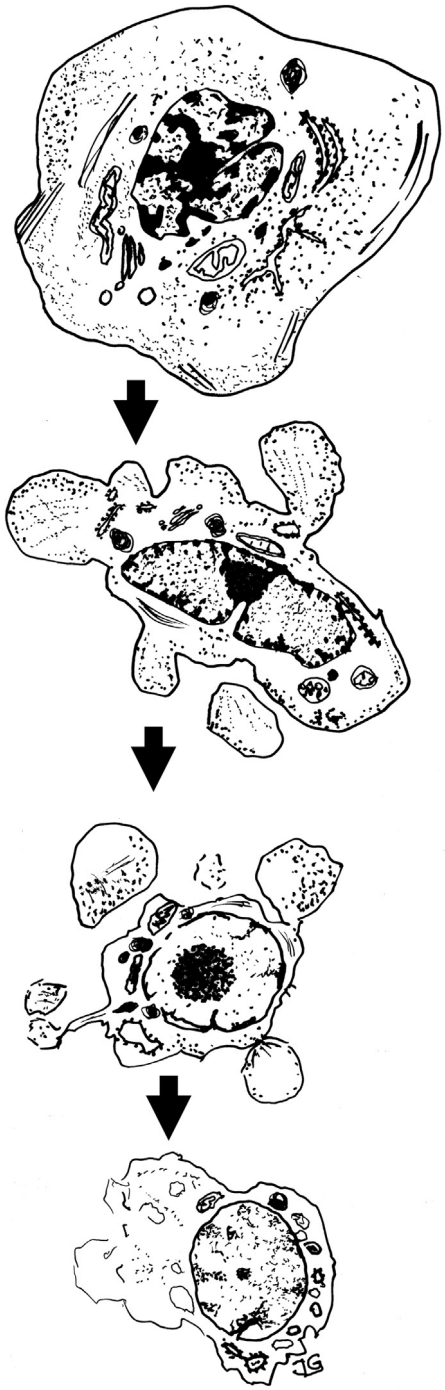

Fig. 11. Diagrammatic representation of a tumor cell undergoing autoschizic cell death.

5. Conclusion

As a combined pro-oxidant the cytotoxic capabilities of the vitamin mixture can kill tumor cells primarily through a new mode of cell death, autoschizis, a process causing irreversible nuclear and cytoplasm injuries that are summarized in Fig. 11.

Altogether, it is quite interesting and important to further enable detecting genetic markers as soon as possible in blood tests among these ovarian tumor types as early as possible because the tumor metabolomics heterogeneity may be important to treat patients with a more 'personalized treatment' [68,73]. Even though some genetic efforts have been not so promising [111], new potential successes could be involving microRNAs [112]. However, and in the meantime, a safe and inexpensive anticancer treatment is still lacking. That is why one can propose that, based on the data submitted, along with those of our late colleague [24], Apatone® treatment may, in the meantime, assists in several stages of patient treatment.

Conflict of interest

There is no conflict of interest.

Acknowledgments

Authors wish to thank IC Med Tech, San Diego, CA, Summa Research Foundation, Akron OH, a grant from the American Institute for Cancer Research, Washington, DC and St George's University School of Medicine. Part of this work was presented by JG as invited speaker at the Anticancer Drug International Meeting, Stockholm, Sweden 22–23 August 2013. Both H.L. Lee and I. Gourari, currently senior medical students, contributed to parts of this report in their scholarly activities at the end of their junior year of study. The work dedicated to the memory of our late colleague and friend Henryk S, Taper, MD, PhD.

References

[1] R.L. Siegel, K.D. Miller, A. Jemal, Cancer statistics, 2015, CA Cancer J. Clin. 65 (2015) 5–29.
[2] A. Jemal, T. Murray, A. Samuels, A. Ghafoor, E. Ward, M. Thun, Cancer statistics, 2003, CA Cancer J. Clin. 53 (2003) 5–26.
[3] C. Sperling, M. Calundann Noer, I.J. Christensen, M.L.S. Nielsen, O. Lidegaard, C. Hogdall, Comorbidity is an independent prognostic factor for the survival of ovarian cancer: a Danish register-based cohort study from clinical database, Gynecol. Oncol. 129 (2013) 97–102.
[4] J.K. Chan, R. Urban, M.K. Cheung, K. Osann, J.Y. Shin, A. Husain, N.N. Teng, D.S. Kapp, J.S. Berek, G.S. Leiserowitz, Ovarian cancer in younger vs older women: a population-based analysis, Br. J. Cancer 95 (2006) 1314–1320.
[5] G. Chornokur, E.K. Amankwah, J.M. Schildkraut, C.M. Phelan, Global ovarian cancer health disparities, Gynecol. Oncol. 129 (2013) 258–264.
[6] B.W. Stewart, C.P. Wild, World Cancer Report 2014 IARC. International Agency for Research on Cancer (IARC), WHO Press, Lyons: France, 2014.
[7] J. Gilloteaux, J.M. Jamison, D. Arnold, J.L. Summers, Human prostate DU145 carcinoma cells implanted in nude mice remove the peritoneal mesothelium to invade and grow as carcinomas, Anat. Rec. A Discov. Mol. Cell Evol. Biol. 296 (2013) 40–55.
[8] T.C. Randall, S.C. Rubin, Cytoreductive surgery for ovarian cancer, Surg. Clin. North Am. 81 (2001) 871–883.
[9] R. Siegel, D. Naishadham, A. Jemal, A Cancer statistics, 2013, CA Cancer J. Clin. 63 (2013) 11–30.
[10] E. Silverberg, J. Lubera, Cancer statistics, 1987, CA Cancer J. Clin. 37 (1987) 2–19.
[11] L.A. Gloecker Ries, Ovarian cancer. Survival and treatment differences by age, Cancer 71 (1993) 524–529.
[12] H.E. Averette, M.F. Janicek, H.R. Menck, The national cancer data base report on ovarian cancer, Cancer 76 (1995) 1096–1103.
[13] J. Gilloteaux, J.M. Jamison, E. Ervin, H.S. Taper, J.L. Summers, SEM and TEM aspects of the synergistic antitumor activity of vitamin C/vitamin K3 combinations against human T24 bladder carcinoma: another kind of cell death? Scanning 20 (1998) 208–210.
[14] J. Gilloteaux, J.M. Jamison, D. Arnold, H.S. Taper, J.L. Summers, Ultrastructural aspects of autoschizis: a new cancer cell death induced by the synergistic

action of ascorbate/menadione on human bladder carcinoma cells, Ultrastruct. Pathol. 25 (2001) 183–192.
[15] J. Gilloteaux, J.M. Jamison, D. Arnold, V.E. von Greuningen, J.L. Summers, Autoschizic death of human ovarian carcinoma (MDAH 2774) cells: LM and SEM aspects, Microsc. Microanal. 7 (suppl. 2) (2001) 586–587.
[16] J. Gilloteaux, J.M. Jamison, D. Arnold, D. Jarjoura, V.E. von Greuningen, J.L. Summers, Autoschizis of human ovarian carcinoma cells: scanning electron and light microscopy of a new cell death induced by sodium ascorbate: menadione treatment, Scanning 25 (2003) 137–149.
[17] J. Gilloteaux, J.M. Jamison, D. Arnold, H.S. Taper, V.E. von Greuningen, J.L. Summers, Microscopic aspects of autoschizic cell death in human ovarian carcinoma (2774) cells following vitamin C, vitamin K3 or vitamin C: K3 treatment, Microsc. Microanal. 9 (2003) 311–329.
[18] J. Gilloteaux, J.M. Jamison, D. Jarjoura, H.E. Lorimer, D.R. Neal, H.S. Taper, J.L. Summers, Autoschizis: a new form of cell death for human ovarian carcinoma cells following ascorbate: menadione treatment. Nuclear and DNA degradation, Tissue Cell 36 (2004) 197–209.
[19] J. Gilloteaux, J.M. Jamison, D. Arnold, J.L. Summers, Autoschizis: another cell death for cancer cells induced by oxidative stress, in: P.M. Motta, G. Machiarelli, S.A. Nottola (Eds.), Advances in Microanatomy of Cells and Tissues, Roma, 2001, pp. 79–91.
[20] J. Gilloteaux, J.M. Jamison, D. Arnold, K. McGuire, M. Loukas, J.P. Sczepaniak, J.L. Summers, Autoschizis : A new cell death induced found in tumour cells induced by oxidative stress mechanism, in: A. Mendez-Villas, J.D. Alvarez (Eds.), Microscopy, Science, Technology, Application and Education, Bajadoz, Spain, Formatex Research Center, Microscopy 1, 2011, pp. 211–220.
[21] H.S. Taper, J.M. Jamison, J. Gilloteaux, C.A. Gwin, T. Gordon, J.L. Summers, In vivo reactivation of DNases in implanted human prostate tumors after administration of a vitamin C/K3 combination, J. Histochem. Cytochem 49 (2001) 109–119.
[22] H.S. Taper, A. Keyeux, M. Roberfroid, Potentiation of radiotherapy by nontoxic pretreatment with combined vitamin C and K3 in mice bearing solid, transplantable tumor, Anticancer Res. 16 (1996) 499–504.
[23] M. Venugopal, J.M. Jamison, J. Gilloteaux, J.A. Koch, M. Summers, D.M. Giammar, C. Sowick, J.L. Summers, Synergistic antitumor activity of vitamin C and K3 on human urologic tumor cell lines, Life Sci. 59 (1996) 1389–1400.
[24] H.S. Taper, Altered deoxyribonuclease activities in cancer cells and its role in non-toxic adjuvant cancer therapy with mixed vitamins C and K3, Anticancer Res. 28 (2008) 2727–2732.
[25] R.S. Freedman, E. Pihl, C. Kusyk, H.S. Gallager, F. Rutledge, Characterization of an ovarian carcinoma cell line, Cancer 4 (1978) 2352–2359.
[26] A.G.E. Pearse, Histochemistry, Theoretical and Applied, fourth ed., Churchill Livingstone, Edinburgh, 1985, pp. 620–656.
[27] S.K. Song, N. Shimada, P.J. Anderson, Orthogonal diameters in the analysis of muscle fiber size and form, Nature 200 (1993) 1220–1221.
[28] R.J. Sambrook, E.F. Fritsch, T. Maniatis, Molecular Cloning, second ed., Cold Spring Harbor Laboratory, Cold Spring Harbor New York, 1989.
[29] M.J. Karnovsky, The ultrastructural basis of capillary permeability studied with peroxidase as a tracer, J. Cell Biol. 35 (1967) 213–236.
[31] I. Persson, Estrogens in the causation of breast, endometrial and ovarian cancers – evidence and hypotheses from epidemiological findings, Steroid Biochem. Mol. Biol. 74 (2000) 357–364.
[32] S. Cunat, P. Hoffmann, P. Oujol, Estrogens and epithelial ovarian cancer, Gynecol. Oncol. 94 (2004) 25–32.
[33] A. Halon, V. Materna, M. Drag-Zelesinska, E. Nawak-Makwitz, T. Gansukh, P. Donizy, M. Spaczynski, M. Zabel, M. Dietel, H. Lage, P. Surowiak, Estrogen receptor alpha expression in ovarian cancer predicts longer overall survival, Pathol. Oncol. Res. 17 (2011) 511–518.
[34] F. Montoya, M. Martin, J. Schneider, J.C. Matia, F.J. Rodriguez-Escudero, Simultaneous appearance of ovarian and endometrial carcinoma: a therapeutic challenge, Eur. J. Gynaecol. Oncol. 10 (1989) 135–139.
[35] M.E. Long, H.C. Taylor, Endometroid carcinoma of the ovary, Am. J. Obstet. Gynecol. 90 (1964) 936–950.
[36] B. Czernoblisky, B.B. Silverman, J.J. Mikuta, Endometroid carcinoma of the ovary. A clinicopathological study of 75 cases, Cancer 26 (1970) 1141–1152.
[37] G. Zampl, M. Colafranceschi, B. Fornari, Endometrioid carcinoma of the ovary: characteristics of form and prognostic significance of the neoplasm, Article in Italian, Arch. De. Vecchi Anat. Patol. 60 (1974) 263–283.
[38] J.E. Wheeler, Pathology of Malignant Ovarian Epithelial Tumors and Miscellaneous and Rare Ovarian and Paraovarian Neoplasms, in: C. Stephen, C. Rubin, G.P. Sutton (Eds.), Ovarian Cancer, McGraw-Hill, Inc., Health Professional Division, New York,, 1993, pp. 87–130. Part 2.
[39] P.A. Cummins, H. Fox, F.A. Langley, An electron-microscopic study of the Endometrioid adenocarcinoma of the ovary and a comparison of its fine structure with that of normal endometrium and of adenocarcinoma of the endometrium, J. Pathol. 113 (1974) 165–173.
[40] A. Blaustein, H. Lee, Surface cells of the ovary and pelvic peritoneum: a histochemical and ultrastructural comparison, Gynecol. Oncol. 8 (1979) 34–43.
[41] C.M. Fenoglio, S. Puri, R.M. Richart, The ultrastructure of endometrioid carcinomas of the ovary, Gynecol. Oncol. 6 (1978) 152–164.
[42] K.C. Choi, N. Auersperg, 2003. The ovarian surface epithelium: simple source of a complex disease, Minerva Gynecol. 55 (2003) 297–314.
[43] R.E. Scully, Ovarian tumors. A review, Am. J. Pathol. 87 (1977) 686–720.
[44] S.F. Lax, R.J. Kurman, A dualistic model for endometrial carcinogenesis based on immunohistochemical and molecular genetic analyses, Verh. Dtsch. Ges. Pathol. 81 (1997) 228–232.
[45] X. Jiang, S.J. Morland, A. Hitchcock, E.J. Thomas, I.G. Campbell, Allelotyping of endometriosis with adjacent carcinomas reveals evidence of a common lineage, Cancer Res. 58 (1998) 1707–1712.
[46] K.M. Feeley, M. Wells, Precursor lesions of ovarian epithelial malignancy, Histopathology 29 (2001) 87–95.
[47] A.H. Prowse, S. Manek, R. Varma, J. Liu, A.K. Godwin, E.R. Maher, I.P. Tomlinson, S.H. Kennedy, Molecular genetic evidence that endometriosis is a precursor of ovarian cancer, Int. J. Cancer 119 (2006) 556–562.
[48] M. Scott, W.G. McCluggage, Current concepts in ovarian epithelial tumorigenesis: correlation between morphological and molecular data, Histol. Histopathol. 21 (2006) 81–92.
[49] F.S. Liu, Molecular carcinogenesis of endometrial cancer, Taiwan J. Obstet. Gynecol. 46 (2007) 26–32.
[50] C.J. O'Neill, W.G. McCluggage, P16 expression in the female genital tract and its value in diagnosis, Adv. Anat. Pathol.13 (2006) 8–15.
[51] R.E. Scully, G.S. Richardson, J.F. Barlow, The development of malignancy in endometriosis, Clin. Obstet. Gynecol. 9 (1966) 384–411.
[52] R. Vang, A.M. Gown, M. Farinola, T.S. Barry, D.T. Wheeler, A. Yemelyanova, J.D. Seidman, K. Judson, B.M. Ronnett, P16 expression in primary ovarian mucinous and endometrioid tumors and metastatic adenocarcinomas in the ovary: utility for identification of metastatic HPV-related endocervical adenocarcinomas, Am. J. Surg. Pathol. 31 (2007) 653–663.
[53] P. Surowiak, V. Materna, A. Maciejczyk, M. Pudelko, S. Suchocki, W. Kedzia, E. Nowak-Markwitz, M. Dumanska, M. Spaczynski, M. Zabel, M. Dietel, H. Lage, Decreased expression of p16 in ovarian cancers represents an unfavourable prognostic factor, Histol. Histopathol. 23 (2008) 531–538.
[54] M. Määttä, R. Bützow, J. Luostarinen, N. Petäjäniemi, T. Pihlajaniemi, S. Salo, K. Miyazaki, H. Autio-Harmainen, I. Virtanen, Differential expression of laminin isoforms in ovarian epithelial carcinomas suggesting different origin and providing tools for differential diagnosis, J. Histochem Cytochem 53 (2005) 1293–1300.
[55] D.J. Dabbs, K. Sturtz, R.J. Zaino, The immunohistochemical discrimination of endometrioid adenocarcinomas, Hum. Pathol. 27 (1996) 172–177.
[56] B. Davidson, W.H. Gotlieb, G. Ben-Baruch, J.M. Nesland, M. Bryne, I. Goldbertg, J. Kopolovic, A. Berner, E-cadherin complex protein expression and survival in ovarian carcinoma, Gynecol. Oncol. 79 (2000) 362–371.
[57] R. Wu, Y. Zhai, E.R. Fearon, K.R. Cho, Diverse mechanisms of beta-catenin deregulation in ovarian endometrioid adenocarcinomas, Cancer Res. 62 (2001) 8247–8255.
[58] C. Wu, C.J. Cipollone, S. Maines-Bandiera, C. Tan, A. Karsan, N. Auersperg, C.D. Roskeley, The morphogenic function of E-cadherin-mediated adherens junctions in epithelial ovarian carcinoma formation and progression, Differentiation 76 (2008) 193–205.
[59] P.T. Soliman, B.M. Slomovitz, R.R. Broaddus, C.C. Sun, J.C. Oh, P.J. Eifel, D.M. Gershenson, K.H. Lu, Synchronous primary cancers of the endometrium and ovary: a single institution review of 84 cases, Gynecol. Oncol. 94 (2004) 456–462.
[60] S.V. Nicosia, R.F. Nicosia, Neoplasms of the Ovarian Mesothelium, in: H.E. Azzar (Ed.), Pathology of Human Neoplasms, Raven Press, New York, 1998, pp. 435–486.
[61] C.O. Granai, All by itself, Gynecol. Oncol. 101 (2006) 1–3.
[62] I. Haviv, I.G. Campbell, DNA microarrays for assessing ovarian cancer gene expression, Mol. Cell Endocrinol. 191 (2002) 121–126.
[63] K.K. Zorn, T. Bonome, L. Gangi, V.R. Chandramouli, C.S. Awtrey, G.J. Gardner, J.C. Barrett, J. Boyd, M.J. Birrer, Gene expression profiles of serous, endometrioid, and clear cell subtypes of ovarian and endometrial cancer, Clin. Cancer Res. 11 (2005) 6422–6430.
[64] P.A. Konstantinopoulos, Gene-expression profiling in epithelial ovarian cancer, Nat. Clin. Pract. Oncol. 5 (2008) 577–587.
[65] M. Huang, C. Page, K.R. Reynolds, J. Lin, Constitutive activation of stat 3 oncogene product in human ovarian carcinoma cells, Gynecol. Oncol. 79 (2000) 67–73.
[66] D.M. Dinulescu, T.A. Ince, B.J. Quade, S.A. Shafer, D. Crowley, T. Jacks, Role of K-ras and PTEN in the development of mouse models of endometriosis and endometrioid ovarian cancer, Nat. Med. 11 (2005) 63–70.
[67] R.J. Kurman, J.M. Craig, Endometrial and clear cell carcinoma of the ovary, Obstet. Gynecol. 27 (1996) 850–858.
[68] A.-M. Patch, E.I. Christie, D. Etermadmoghadam, et al., Whole-genome characterization of chemoresistant ovarian cancer, Nature 521 (2015) 489–494.
[69] B.Y. Karlan, J.L. Jones, M. Greenwaild, L.D. Lagasse, Steroid hormone effects on the proliferation of human ovarian surface epithelium in vitro, Am. J. Obstet. Gynecol. 173 (1995) 97–104.
[70] M.K Lau, S.C. Mok, S.M. Ho, Expression of human estrogen receptor-α and -ß, progesterone receptor, and androgen receptor mRNA in normal and malignant ovarian epithelial cells, Proc. Natl. Acad. Sci. U. S. A. 96 (1999) 5722–5727.
[71] L. Dubeau, Pathogenesis of serous, extra-uterine Müllerian epithelial cancer and therapeutic implications, Transl. Cancer Res. 4 (2015) 30.
[72] I. Harley, B. Rosen, H.A. Risch, K. Siminovitch, M.E. Beiner, J. McLaughlin, et al., Ovarian cancer risk is associated with a common variant in the promoter sequence of the mismatch repair gene MLHI\1, Gynec Oncol. 109 (2006)

384–387.
[73] L. Beltrame, M. Di Marino, R. Fruscio, E. Calura, B. Chapman, L. Clivio, F. Sina, et al., Profiling cancer gene mutations in longitudinal epithelial ovarian cancer biopsies by targeted next-generation sequencing: a retrospective study, Ann. Oncol. (2015). April 6, pii: mdv164.
[74] H.S. Taper, La détection histochimique de la désoxyribonuncléase alcaline, Ann. Histochim. 13 (1968) 301–317.
[75] L. Fort, H.S. Taper, J.M. Brucher, Nucleases activity in different segments of the human digestive tube compared to the incidence of carcinomas (histochemical study), Histochemie 20 (1969) 150–158.
[76] H.S. Taper, The relation between the histochemical activity of nucleases and neoplasms in rat and man, Thesis, Vander Publisher: Louvain, Belgium, 1975, pp. 1–198. pp. i-vii.
[77] H.S. Taper, J. de Gerlache, M. Lans, M. Roberfroid, Non-toxic potentiation of cancer chemotherapy by combined C and K3 vitamin pretreatment, Int. J. Cancer 40 (1987) 575–579.
[78] H.S. Taper, M. Roberfroid, Non-toxic sensitization of cancer chemotherapy by combined C and K3 vitamin pretreatment in a mouse tumor resistant to oncovin, Anticancer Res. 12 (1992) 1651–1654.
[79] H.S. Taper, J.M. Jamison, J. Gilloteaux, J.L. Summers, P.B. Calderon, Inhibition of the development of metastases by dietary vitamin C: K3 combination, Life Sci. 75 (2004) 955–967.
[80] J. Gilloteaux, A.W. Steggles, Histoenzymatic alterations in kidney catalase activity following hormonal treatment of Syrian hamster, Cell Biol. Int. Rep. 7 (1983) 31–33.
[81] S. Cablé, J.M. Keller, S. Colin, K. Haffen, M. Kédinger, R.M. Parache, M. Dauca, Peroxisomes in human colon carcinomas. A cytochemical and biochemical study, Virchows Arch. B Cell Pathol. Mol. Pathol. 62 (1992) 221–226.
[82] J.M. Keller, S. Cablé, F. el Bouhtoury, S. Heusser, C. Scotto, E. Armbruster-Ciolek, S. Colin, J. Schilt, M. Dauca, Peroxisome through cell differentiation and neoplasia, Biol. Cell 77 (1993) 77–88.
[83] C. Lauer, A. Völkl, S. Riedl, H.D. Fahimi, K. Beier, Impairment of peroxisomal biogenesis in human colon carcinoma, Carcinogenesis 20 (1969) 985–989 and Erratum in: Carcinogenesis 20(1999) 2037.
[84] W.M. Fredericks, H. Vreeling-Sindelárová, C.J. Van Noorden, Loss of peroxisomes causes oxygen insensitivity of the histochemical assay of glucose-6-phosphate dehydrogenase activity to detect cancer cells, J. Histochem Cytochem 55 (2007) 175–181.
[85] V. Noto, H.S. Taper, Y.H. Jiang, J. Janssens, J. Bonte, W. De Loecker, Effects of sodium ascorbate (vitamin C) and 2-methyl-1, 4-naphthoquinone (vitamin K3) treatment on human tumor cell growth in vitro. I. Synergism of combined vitamin C and K3 action, Cancer 63 (1989) 901–906.
[86] W. DeLoecker, J. Janssens, J. Bonte, H.S. Taper, Effects of sodium ascorbate (vitamin C) and 2-methyl-1, 4-naphtoquinone (vitamin K3) treatment on human tumor cell growth in vitro. II. Synergism with combined chemotherapy action, Anticancer Res. 13 (1993) 103–106.
[87] J. Verrax, J. Carobbi, M. Delvaux, J.M. Jamison, J. Gilloteaux, J.L. Summers, H.S. Taper, P.B. Calderon, The association of vitamins C and K3 kills cancer cells mainly by autoschizis, a novel form of cell death. Basis for their potential use as coadjuvants in anticancer therapy, Eur. J. Med. Chem. 38 (2003) 451–457.
[88] J. Verrax, J. Cadrobbi, C. Marques, H.S. Taper, Y. Habraken, J. Piette, P.B. Calderon, Ascorbate potentiates the cytotoxicity of menadione leading to an oxidative stress that kills cancer cells by a non-apoptotic caspase-3 independent form of cell death, Apoptosis 9 (2004) 223–235.
[89] R. Daoust, H. Amano, Improved DNA film method for localizing DNAse activity in tissue sections, Exp. Cell Res. 24 (1961) 559–564.
[90] A. Begleiter, Cytocidal action of the quinone group and its relationship to antitumor activity, Cancer Res. 43 (1983) 481–484.
[91] D. Carbonera, G.F. Azzone, Permeability of inner mitochondrial membrane and oxidative stress, Biochim. Biophys. Acta 943 (1988) 245–255.
[92] J.M. Jamison, J. Gilloteaux, H.S. Taper, P.B. Calderon, L. Perlaky, M. Thiry, D.R. Neal, J.L. Blank, R.J. Clements, S. Getch, J.L. Summers, The in vitro and in vivo antitumor activity of vitamin C: K3 combinations against prostate cancer, Chapter VII, in: John N. Lucas (Ed.), Trends in Prostate Cancer Research. Nova Science Publishers, Inc. Hauppauge New York, 2005, pp. 189–236.
[93] M. Venugopal, J.M. Jamison, J. Gilloteaux, J. Koch, M. Summers, J. Hoke, C. Sowick, J.L. Summers, Synergistic antitumor activity of vitamins C and K3 against human prostate carcinoma cell lines, Cell Biol. Intl 20 (1996) 787–797.
[94] J.M. Jamison, J. Gilloteaux, M. Venugopal, J.A. Koch, C. Sowick, R. Shah, J.L. Summers, Flow cytometric and ultrastructural aspects of the synergistic antitumor activity of vitamin C-vitamin K3 combinations against prostatic carcinoma cells, Tissue Cell 28 (1996) 687–701.
[95] J.M. Jamison, J. Gilloteaux, M.R. Nassiri, M. Venugopal, D.R. Neal, J.L. Summers, Cell cycle arrest and autoschizis in a human bladder carcinoma cell line following vitamin C and vitamin K3 treatment, Biochem. Pharmacol. 67 (2004) 337–351.
[96] R. Pething, P.R.C. Gascoyne, J.A. McLaughlin, A. Szent-Györgyi, Ascorbate-quinone interactions: electrochemical, free radical and cytotoxic properties, Proc. Natl. Acad. Sci. U. S. A. 80 (1983) 129–132.
[97] R. Jarabak, J. Jarabak, Effect of ascorbate on the DT-diaphorase mediated redox cycling of 2-methyl-1,4-naphtoquinone, Arch. Biochem. Biophys. 318 (1995) 418–423.
[98] G.R. Buettner, B.A. Jurkewicz, Catalytic metals, ascorbate and free radicals: combinations to avoid, Radiat. Res. 145 (1996) 532–541.
[99] G. Silviera-Dorta, D.M. Monzon, F.P. Crisostomo, T. Martin, V.S. Martin, R. Carrillo, Oxidation with air by ascorbate-driven quinone redox cycling, Chem. Commun. 51 (2015) 7027–7030.
[100] G. Cantuaria, A. Fagotti, G. Ferrandina, A. Magalhaes, M. Nadji, R. Angioli, M. Penalver, S. Mancuso, G. Scambia, GLUT-1 expression in ovarian carcinoma, Cancer 92 (2001) 1144–1150.
[101] W. Zhang, T. Negoro, K. Satoh, Y. Jiang, K. Hashimoto, H. Kikuchi, H. Nishikawa, T. Miyata, Y. Yamamoto, K. Nakano, E. Yasumoto, T. Nakayachi, K. Mineno, T. Satoh, H. Sakagami, Synergistic cytotoxic action of vitamin C and vitamin K3, Anticancer Res. 21 (2001) 3439–3944.
[102] M.M. Myat, S. Anderson, L.A. Allen, M.A. Myat, MARCKS regulates membrane ruffling and cell spreading, Curr. Biol. 7 (1997) 611–614.
[103] J.M. Jamison, J. Gilloteaux, L. Perlaky, M. Thiry, K. Smetana, D. Neal, K. McGuire, J.L. Summers, Nucleolar changes and fibrillarin redistribution following Apatone treatment of human bladder carcinoma cells, J. Histochem Cytochem 58 (2010) 635–651.
[104] J. Gilloteaux, J.M. Jamison, D. Arnold, D.R. Neal, J.L. Summers, Morphology and DNA degeneration during autoschizic.cell death in bladder carcinoma T24 cells induced by ascorbate and menadione treatment, Anat. Rec. A Discov. Mol. Cell Evol. Biol. 88 (2006) 58–83.
[105] K. McGuire, J.M. Jamison, J. Gilloteaux, J.L. Summers, Vitamin C and K3 combination causes enhanced anticancer activity against RT-4 bladder cancer cells, J. Cancer Sci. Ther. 4 (2013) 7–19.
[106] J. Gilloteaux, J.M. Jamison, D.R. Neal, J.L. Summers, Synergistic antitumor cytotoxic actions of ascorbate and menadione on human prostate (DU145) cancer cells in vitro: nucleus and other injuries preceding cell death by autoschizis, Ultrastruct. Pathol. 38 (2014) 116–140.
[107] J. Gilloteaux, J.M. Jamison, J.L. Summers, Pro-oxidant treatment of human prostate carcinoma (DU145) cells induces autoschizis cell death: Autophagosomes build up out of injured endomembranes and mitochondria, Ultrastruct. Pathol. 38 (2014) 315–328.
[108] J. Gilloteaux, J.M. Jamison, D.R. Neal, M. Loukas, T. Doberzstyn, J.L. Summers, Cell damage and death by autoschizis in human bladder (RT4) carcinoma cells resulting from treatment with ascorbate and menadione, Ultrastruct. Pathol. 34 (2010) 140–160.
[109] J. Gilloteaux, J.M. Jamison, M. Venugopal, D. Giammar, J.L. Summers, Scanning electron microscopy and transmission electron microscopy aspects of synergistic antitumor activity of vitamin C – vitamin K3 combinations against human prostatic carcinoma cells, Scanning Microsc. 9 (1995) 159–173.
[110] J. Gilloteaux, J.M. Jamison, D. Arnold, J.L. Summers. Autoschizis: a mode of cell death of cancer cells induced by a pro-oxidant treatment in vitro and in vivo, in: Apoptosis and Other Cell Deaths. J. Radovich (ed.), Springer Verlag, New York-Heidelberg. In press.
[111] O. Gevaert, F. De Smet, T. Van Gorp, N. Pochet, K. Engelen, F. Amant, B. De Moor, D. Timmerman, J. Vergote, Expression profiling to predict the clinical behaviour of ovarian cancer fails independent evaluation, BMC Cancer 22 (2008) 8–18, http://dx.doi.org/10.1186/1471-2407-8-18.
[112] A. Semaan, A.M. Qazi, S. Seward, S. Chamala, C.S. Bryant, S. Kumar, R. Morris, C.P. Steffes, D.L. Bouwman, A.R. Munkarah, D.W. Weaver, S.A. Gruber, R.B. Batchu, MicroRNA-101 inhibits growth of epithelial ovarian cancer by relieving chromatin-mediated transcriptional repression of p21(waf^1/cip^1), Pharm. Res. 8 (2011) 3079–3090.